NOV 2 9 1994

ORNL/NRC/LTR-94/26

ORNL
MASTER COPY

Contract Program or Project Title:	Heavy-Section Steel Technology (HSST) Program, Metals and Ceramics Division
Subject of this Document:	Assessment of Metallurgical Effects that Impact Pressure Vessel Safe Margin Issues
Type of Document:	Letter Report
Authors:	D. E. McCabe
Date of Document	October 1994
Responsible NRC Individual and NRC Office or Division:	S. N. M. Malik (301-415-6007) Division of Engineering, U.S. Nuclear Regulatory Commission

Prepared for the
U.S. Nuclear Regulatory Commission
Washington, DC 20553
Under Interagency Agreement DOE 1886-8011-9B
NRC JCN No. B0119

OAK RIDGE NATIONAL LABORATORY
Oak Ridge, TN 37831-6151
managed by
MARTIN MARIETTA ENERGY SYSTEMS, INC.
for the
U.S. Department of Energy
under Contract No. DE-AC05-84OR21400

ORNL/NRC/LTR-94/26

ASSESSMENT OF METALLURGICAL EFFECTS THAT IMPACT PRESSURE VESSEL SAFE MARGIN ISSUES

D. E. McCabe

Manuscript Completed - September 1994
Date Published - October 1994

Prepared for the
U.S. Nuclear Regulatory Commission
Washington, DC 20553
Under Interagency Agreement DOE 1886-8011-9B

NRC JCN No. B0119

Prepared by the
OAK RIDGE NATIONAL LABORATORY
Oak Ridge, TN 37831-6151
managed by
MARTIN MARIETTA ENERGY SYSTEMS, INC.
for the
U.S. Department of Energy
under Contract No. DE-AC05-84OR21400

CONTENTS

ABSTRACT 1
INTRODUCTION 1
POP-INS 2
DISCUSSION - POP-INS 7
CLADDING EFFECTS 10
DISCUSSION - CLADDING EFFECTS 19
WARM PRESTRESS 19
DISCUSSION - WARM PRESTRESS 24
TRANSITION TEMPERATURE TOUGHNESS 25
DISCUSSION - TRANSITION TEMPERATURE TOUGHNESS 28
STRAIN RATE EFFECTS 32
DISCUSSION - STRAIN RATE EFFECTS 41
SUMMARY 41
ACKNOWLEDGMENTS 43
REFERENCES 43

ASSESSMENT OF METALLURGICAL EFFECTS THAT IMPACT PRESSURE VESSEL SAFE MARGIN ISSUES

D. E. McCabe

ABSTRACT

The purpose of this letter report is to develop viewpoints from experimental work that might have some impact on low-temperature overpressurization protection (LTOP) issues. The allowed pressure/temperature window for safe startup and shutdown of reactors has been approaching untenable limits in several operating nuclear installations. Large factors of safety that were easily accommodated at the beginning of life are now asserting penalties that may force the retirement of perfectly safe units. Hence, the time has come to consider modifications to LTOP limits if the changed policy can be justified through supporting data and newer technical developments. One proposed revision under consideration is to replace the dynamic K_{IR} curve with the static lower-bound K_{Ic} curve, which would result in a 35°C opening of the allowed pressure/temperature window. This report presents recent information relating to the transition temperature range fracture toughness characterization of pressure vessel steels. The subjects addressed are (1) the relevance of the crack pop-in phenomenon, (2) the effect of cracks in cladding, (3) the potential benefit of warm prestress effects, and (4) new information relevant to the accurate location of both static and dynamic fracture toughness transition curves.

INTRODUCTION

The American Society of Mechanical Engineers (ASME) Section XI Task Group on Reactor Vessel Integrity Requirements has taken the position that Appendix G of the *ASME Boiler and Pressure Vessel Code* should be reviewed and updated to reflect current technical knowledge.[1] In particular, the bases for the establishment of safe operating margins, for example, low-temperature overpressurization (LTOP) protection for level A and B transients and pressurized thermal shock conditions were recommended for reevaluation. With many operating plants near the end of life, generous original factors of safety established on the basis of unmatured technologies could result in the unnecessary termination of operation for plants that could actually be perfectly safe.[2] Because of the high initial material toughness of typical reactor vessel steels, most LTOP transient pressure/temperature operating windows were set with wide safety margins when plants were new. However, with service and consequent irradiation embrittlement of pressure vessels, especially those with high copper and nickel weld joints, there are now a number of operating units facing difficult transient control problems.

To broaden the LTOP operating windows, one helpful step would be to justify the replacement of the dynamic K_{IR} transition range fracture toughness versus temperature curve with the static lower-bound K_{Ic} curve. The LTOP condition involves essentially static loading, but, to justify the replacement of the dynamic toughness curve with a

static curve, it is necessary to prove that there is no possibility of a running cleavage crack being introduced that would require the crack-arrest capability represented by the K_{IR} fracture toughness.

Developments in technical information resources have been of two types: (1) improved crack driving force analyses (analytical), and (2) improved identification of the metallurgical conditions that could lead to uncontrolled brittle running cracks. Only the metallurgical aspects will be covered in this report. Specific subjects to be addressed are: (1) introduction of running cracks from cleavage crack pop-in sources, (2) evaluation of the effect of stainless cladding on fracture toughness performance of the reactor vessel, (3) potential benefit of warm prestress effects, (4) identification of the ductile-to-brittle transition temperature, and (5) revisiting the effect of strain rate on the transition temperature.

POP-INS

Crack pop-ins are crack initiation and arrest events that have been observed in fracture mechanics type test specimens and in thermal shock experiments of intermediate size pressure vessels.[3] Crack arrest of a pop-in is caused by either diminished crack driving force with crack enlargement or by the running crack encountering a region of higher crack-arrest fracture toughness. Pop-ins were commonly observed in early fracture mechanics testing experiences with aerospace materials.[4] These materials are highly frangible with little to no strain rate sensitivity and crack arrest came from low crack initiation, K_I, coupled with reduced crack driving force with crack size enlargement. Pop-ins and complete brittle fractures were the very first criteria used to identify the K_{Ic} fracture toughness.[5] In structural configurations, pop-ins are most often observed in weldments containing brittle weld beads and/or embrittled heat-affected zone (HAZ) material. Pop-in initiation comes from cracks in the embrittled material caused by either hydrogen embrittlement or reheat processing. Generally, brittle weld beads and cracks develop because mistakes have been made in the welding practice and these problems are exacerbated by a lack of postweld heat treatment (PWHT).[6] Irradiation is not likely to improve the fracture toughness of brittle weld bead materials so that the control of cleavage crack propagation then depends upon the superior toughness of the surrounding crack-arrest material. The K_R curve toughness property of base metal is the line of defense that controls safe performance in such cases. It should be mentioned, however, that postulated lack of PWHT is an improbable scenario for reactor beltline weld materials.

A subcategory of embrittled HAZ material is termed "local brittle zone" (LBZ). Local brittle zones have been discovered in heat-affected zones of multipass weldments in the form of a thin highly discontinuous coarse grain layer along the fusion line, as shown schematically in Fig. 1. These are observed most commonly in multipass welds of microalloyed steels and in applications where stress relief anneal is not applied. The embrittled material is nominally about 0.08 mm thick (0.003 in.) and

ORNL-DWG 90-6431

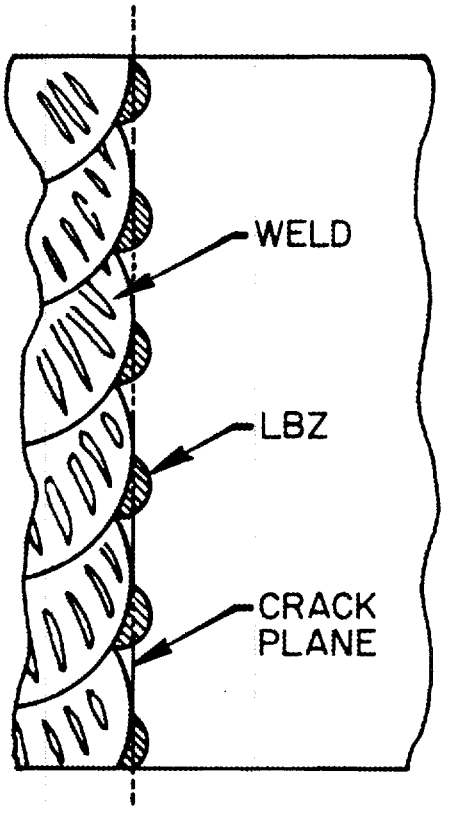

Fig. 1. Schematic of local brittle zones in a multipass weld.

discontinuous to the extent that fracture toughness specimens carefully positioned to locate the crack tip in the plane of LBZ material will usually have only 5 to 25% LBZ material along the crack front. With a well-chosen test temperature and a carefully positioned specimen, it is possible to demonstrate either pop-in and/or full cleavage behavior.[7] The interesting perspective on LBZ studies is that special welding techniques are usually required to create local brittle zones. Postweld heat treatment is to be avoided. In addition, the LBZ fracture phenomenon has been identified almost entirely in test specimens. Investigators who have devoted considerable effort to studying the LBZ effect have not been able to clearly cite any instances in which the phenomenon has caused a major structural failure problem.[8,9] On the other hand, pop-ins from the previously mentioned brittle weld bead metals with macroscale surface cracks due to heat-treatment and/or hydrogen embrittlement have clearly been associated with serious structural failures.[10]

Pop-ins have also been observed in tests of monolithic materials such as base metals. Pop-in and full cleavage fractures intermix among replicate tests with the pop-ins having a very low frequency of occurrence. Plates and forgings of structural steels in their typical commercial heat-treated conditions rarely display crack pop-ins. These materials usually have strain rate sensitivity and there will be a significant separation between crack initiation and crack-arrest toughness versus temperature transition curves. As a consequence, once initiated, assuming uniform stress and temperature, a running crack is not likely to be arrested.

Under certain conditions, however, frequency of pop-in occurrences in monolithic materials can be high. Monolithic in this context refers to the condition under which mechanical properties in the crack tip region are, for all intents and purposes, relatively uniform. This might include the midplane of weld metals as well as base metals. Such materials can display pop-in behavior within a range of test temperatures in the transition range if the strain rate sensitivity is conducive to creating the pop-in phenomenon. Usually a certain degree of embrittlement is needed to optimize the crack initiation and crack-arrest transition range toughness balance that is needed. The Heavy-Section Steel Irradiation (HSSI) Program Fifth Irradiation Series[11] on A 533 grade B submerged-arc weld metals has provided an excellent example. The test specimens were compact-type, ranging in size from 1T to 8T. Of 155 unirradiated specimens tested, two had shown relatively small pop-ins in their test records. After an irradiation fluence of 1.5×10^{19} neutrons/cm^2 (>1 MeV) at 288°C (550°F), 29 of 110 specimens tested displayed pop-ins, and, in some of these specimens, there were multiple pop-ins. It was also noted that irradiation caused a 12°C decrease in temperature spread between the static and dynamic toughness versus temperature curves. Using the toughness level of 100 MPa$\sqrt{m}$ as a baseline, the preirradiation spread was 34°C and the postirradiation spread was 22°C. Ostensibly, this reduction in strain rate sensitivity, and a 30% increase in yield strength, promoted the increased propensity for pop-ins. Other identical specimens that failed completely provided an opportunity to evaluate the relevance of pop-ins (see Figs. 2 and 3). First pop-ins

ORNL-DWG 91-14737R2

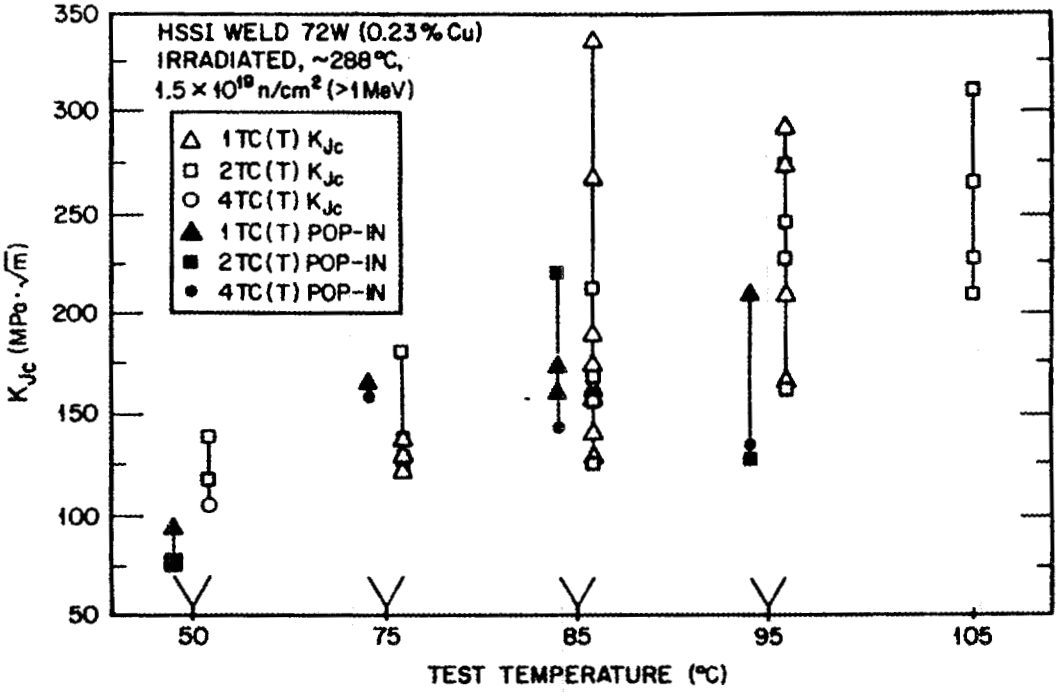

Fig. 2. Cleavage fracture toughness for HSSI irradiated weld 72W, comparing first pop-in events with fracture toughness results. Each datum represents one specimen.

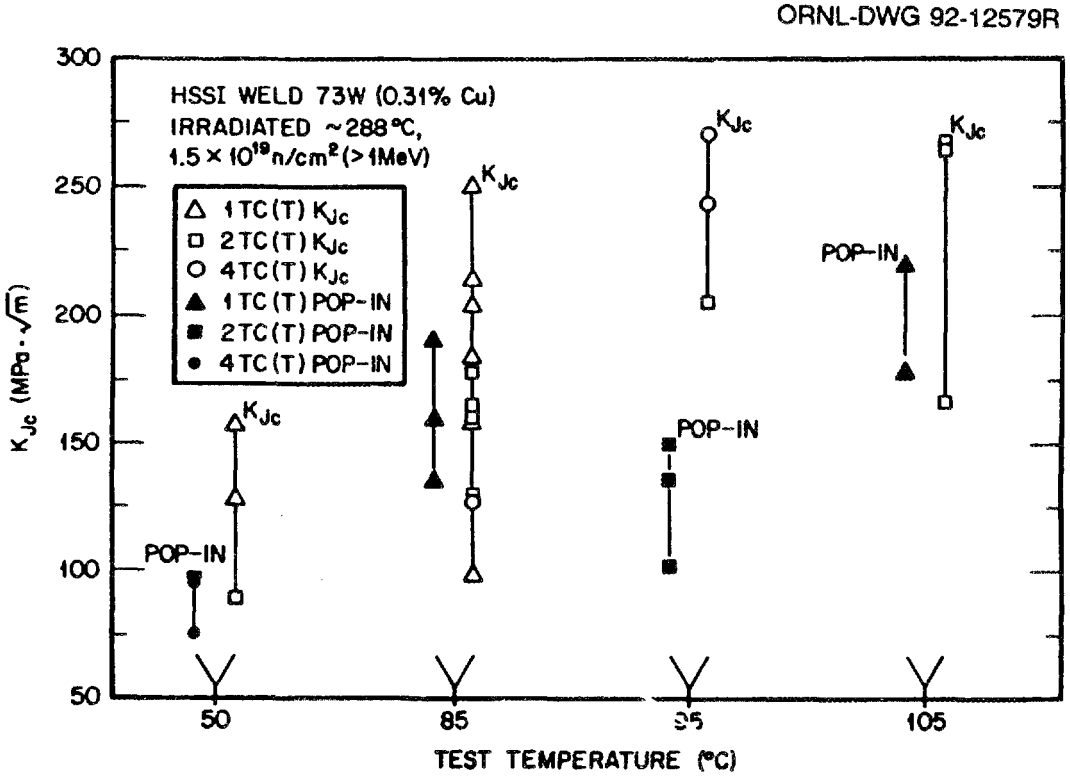

Fig. 3. Cleavage fracture toughness for HSSI irradiated weld 73W, comparing first pop-in events with fracture toughness results. Each datum represents one specimen.

seem to fit for the most part within the scatter band of cleavage instability toughness values. Pop-in events tend to favor the low end of the data scatter, but this is to be expected, considering that a small fracture toughness margin is needed between crack driving force and the crack-arrest toughness capability of the material to create the phenomenon. The increased frequency of pop-ins apparently is promoted by more overlap between K_{Jc} and K_{Ia} data scatter distributions. They are also further aided (to a lesser extent) by the usual test practice of displacement-controlled loading of specimens.

Various working groups within the American Society for Testing and Materials (ASTM) Committee E08 on Fatigue and Fracture have agreed upon a pop-in evaluation procedure. It was decided that a pop-in event can be judged nonsignificant if the indicated crack jump in a test specimen corresponds to less than 2% of the initial crack size. This is measured by a nominal 5% change in compliance that is determined using construction lines drawn on test records. Thus the committee judgment is that there are occasions when apparent cleavage crack initiation can be ignored. Somehow overlooked in these considerations is the fact that a 2% crack jump is a specimen size-dependent criterion. A nonsigifnicant cleavage crack jump in a 4T specimen might be a significant pop-in for a 1T or 2T size specimen (see examples in Figs. 4 and 5). The ASTM rules may be justified when applied to weldments in which the pop-in crack arrests are due to significant fracture toughness gradients. On the other hand, a rule that allows the investigator to ignore pop-ins may not be appropriate for the evaluation of monolithic materials or for reactor safety issues where a lack of assured crack arrest could be catastrophic.

DISCUSSION - POP-INS

The pop-in phenomenon occurs under two generic conditions. The first is in weldments in which pop-ins initiate in brittle weld material and arrest in base metal of higher toughness. The second is in monolithic materials in which the sensitivity of fracture toughness to strain rate is either reduced or absent. Only the latter type of pop-in (monolithic) needs to be considered in reactor vessel safety issues because the weld and base metal properties of reactor pressure vessel steels are usually comparable after ***properly executed*** postweld heat treatment. Pop-ins from local brittle zones that are only postulated to exist in reactor vessel welds are not a proven issue since it has been raised without supporting evidence. Proof of properly executed PWHT should resolve the LBZ issue for reactor vessels currently in operation with many years in service. Pop-ins in monolithic materials appear to be a phenomenon caused by the convergence of static and dynamic fracture toughness curves. At the same time, cleavage crack initiation toughnesses for first pop-ins appear to belong within the data scatter band of static K_{Jc} fracture toughness values. Therefore, when static K_{Jc} data scatter characterizations include first pop-ins as a part of the data population, the issue of pop-ins as a source for dynamic crack introduction can be adequately covered. In this way, the pop-in phenomenon can be disposed of as

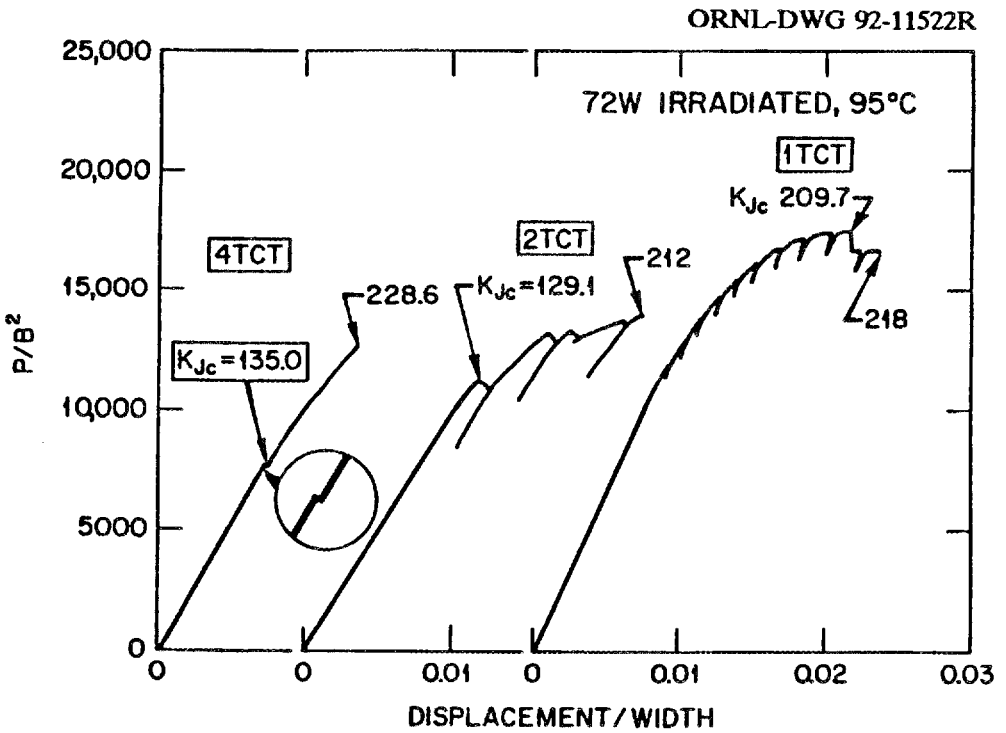

Fig. 4. Test record appearance for 4T, 2T, and 1T compact specimens. Test temperature is 95°C.

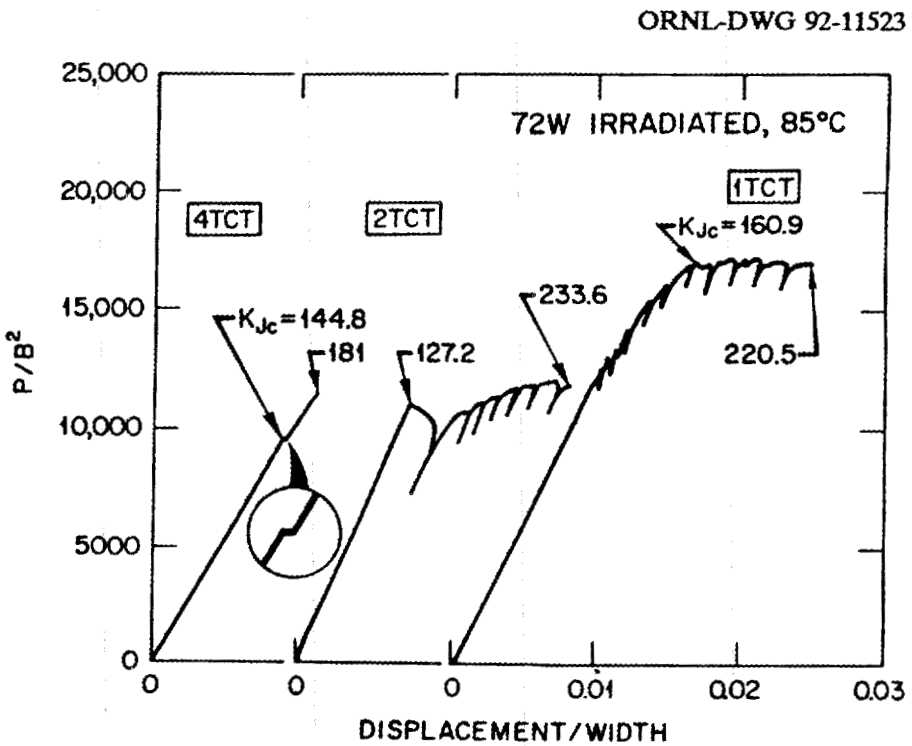

Fig. 5. Test record appearance for 4T, 2T, and 1T compact specimens. Test temperature is 85°C.

a separate issue in the consideration of the replacement of the K_{IR} curve with the K_{Ic} curve for LTOP control.

CLADDING EFFECTS

Advances made on understanding cladding effects have resulted from two technical approaches. One is the development of sophisticated crack driving force solutions using finite-element programs that incorporate the complex multi-region material constitutive properties, residual stress contributions, thermal stress gradients, and constraint phenomena that affect the behavior of small flaws.[12] The second approach is to conduct experiments that directly measure the fracture toughness characteristics for small flaws in various locations within the three materials of the weld bonded region. This involves fracture toughness tests using small semielliptical surface flaws or elliptical embedded flaws in various locations. Only the experimental work is addressed here.

The original purpose for welding stainless cladding to the internal surfaces of reactor vessels and steam generators was to minimize corrosion product buildup in the coolant water. The potential influence of the weld layering on the structural properties was not considered relevant during reactor design. This disinterest in the structural property significance of cladding vanished when small flaws of the order of 3.2 to 9.5 mm deep (0.125 to 0.375 in.) were discovered in the clad layer and in the underlying HAZ.[13] Because flaws embedded entirely in the clad layer are usually quite small, calculated crack driving force under normal operating conditions and for LTOP thermal transients were judged to be of no concern. The current ASME position on such cracks for normal and upset conditions is that they can be regarded as if they are not present. For flaws that penetrate deeper than the clad/base metal interface, advantage can be taken of the lower thermal conductivity of the stainless steel layer, using its beneficial effect in the form of a reduced thermal stress gradient (secondary stress). However, such larger surface flaws that penetrate through the cladding may require more detailed considerations and the total cracked area (including the part in the clad region) needs to be used in the transient condition analyses.[14] The major concern has been crack driving force developed during pressurized thermal shock scenarios during which the potential for cleavage crack introduction into the base metal is much greater. On the other hand, it has also been pointed out that there may be some advantage for subclad cracks having a layer of highly tough material that potentially could exert a mitigating influence on the crack driving force situation. Experiments have been conducted to test this theory.[15-17]

In ref. 15, 51-mm-thick (2-in.) plates of A 533 grade B steel were heat-treated to have a high drop-weight nil-ductility transition (NDT) temperature [36°C (97°F)] in simulation of an irradiation-damaged steel. Some plates were clad layered with combinations of types 308, 309, and 312 stainless steel. The clad plates were then given the usual post cladding stress relief anneal at 607°C (1125°F). All test plates

were 406 mm wide by 94 mm long (16 by 36 in.). Cleavage initiator flaws were inserted into a central unclad area of the plate. These flaws were made by electron-beam (EB) welding relatively deep semielliptical surface crack shapes. The experiment involved preloading the plates to various preselected load levels and then sustaining that load while the EB weld slit was electrolytically hydrogen embrittled until cleavage crack initiation developed. The loading was by four-point bending and test temperatures ranged from 25 to −100°C (75 to −148°F). These tests showed that the cladding process can indeed improve the transition temperature characteristics of the plate with respect to those of base metal. Baseline tests of specimens made of base metal only showed complete brittle fracture at 25°C (75°F). Clad specimen tests showed crack arrest under the clad layer in the form of pop-in behavior between +25 and −25°C (+75 and −13°F). Frequently these same specimens would fracture completely upon continued loading after the pop-in event. At test temperatures of −50°C (−58°F) and below, all specimens failed with no intermediate pop-ins. In addition to the toughness improvement, another observation was that crack-arrest did not seem to occur at the cladding-HAZ interface, but at the HAZ-base metal interface, perhaps 5 mm (0.2 in.) below the clad layer. Evidently the properties of the clad metal itself were not involved in producing the improved toughness behavior observed, because the cladding was shielded by the HAZ. Another evaluation of interest came from the J-R curve toughness testing of specimens made of clad metal only. The measured toughness, shown in Fig. 6, is about the same as that of a low upper-shelf ferritic steel, falling far short of the fracture toughness expectations that typify austenitic stainless steel plate material. This difference is primarily due to cast versus wrought microstructures.

An experiment at Materials Engineering Associates[16] added substantially confirming information to the Oak Ridge National Laboratory (ORNL) work. Here, the transition temperature characteristics for semielliptical surface cracks embedded in the clad layer of bend bar specimens was the criterion of evaluation. Some cracks were initially deep enough to penetrate the clad layer and others extended only to about midthickness of the clad layer. The base metal was A 533 grade B steel and the cladding was applied by a typical commercial three-wire layering process using combinations of types 304 and 308 stainless steel, followed by stress-relief anneal at 607°C (1125°F) for 16 h. The test specimens were four-point loaded beams 50- by 63-mm (2- by 2.5-in.) cross section and 406-mm (16-in.) overall span.

The parameter evaluated was fracture mechanics-based transition temperature. Beams of base metal only and others with cladding were tested in both the as-received condition and after irradiation to 1.5×10^{19} neutrons/cm^2 (>1 MeV) at 288°C (550°F). Also, compact specimens of 1/2T plan view size but 5 mm thick (0.2 in.) were used to characterize the three metallurgical zones (weld metal, HAZ, and base metal) and these were also tested in the as-received and irradiated conditions. The compact specimens demonstrated that the material having the lowest transition temperature (highest toughness) was the HAZ. The base metal had about a 50°C

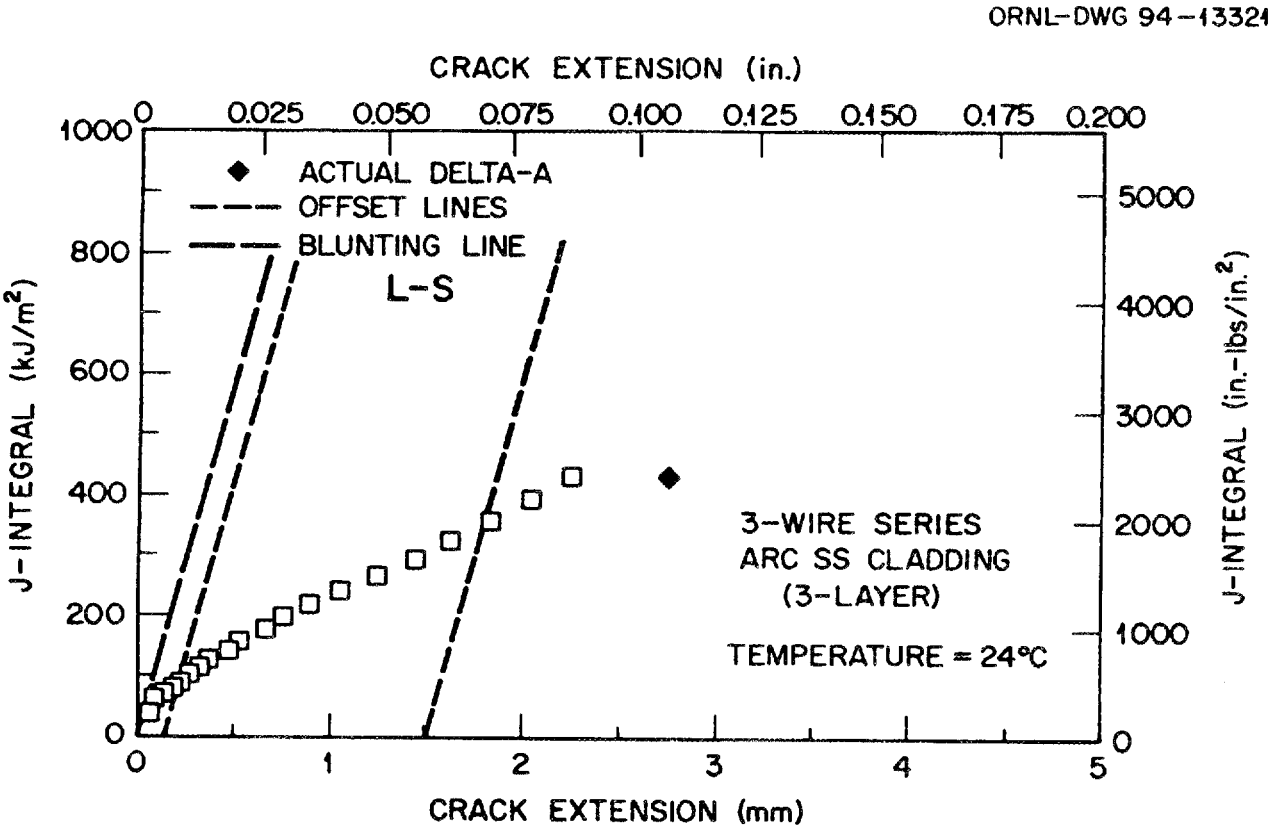

Fig. 6. J-R curve for clad metal developed in the ORNL clad plate experiments.

(90°F) higher transition temperature, based on the temperature separation of the K_{Jc} transition curves at the 100-MPa$\sqrt{m}$ level. The clad metal showed a Charpy impact energy transition temperature (Fig. 7), but the mechanism was not a cleavage-related phenomenon. Rather, it was determined to be a phenomenon of changed resistance to slow-stable crack growth, as shown in Fig. 8. At upper-shelf temperatures, the tearing resistance (J-R curve) is no better than that of a low upper-shelf pressure vessel steel. At the lower temperatures at which some of the surface-cracked bend bar tests were made, the ductile tearing resistance is quite low.

The K_{Jc} instability fracture toughness values from the bend-bar tests are plotted as data points in Fig. 9 along with the solid line HAZ and base metal transition curves previously developed with compact specimens. The data points are for both flaw sizes. For the tests that were stopped before cleavage instability failure, the K_J values at test termination are shown as open points. Note that there is a distinct tendency for the bend-bar data to follow the HAZ transition temperature curve, except for one small flaw datum at −125°C. This test was purposely terminated prior to cleavage fracture so that the crack could be marked by heat tinting and then examined after being broken open. The crack was found to have grown, but to a point short of the HAZ. In this one case the ductile tearing within the clad metal had shielded the underlying HAZ material from brittle fracture. Cleavage fracture by HAZ material evidently does not occur until the crack actually reaches the clad-HAZ fusion line. This was taken as evidence that cleavage instability from surface cracks in cladding is controlled by the HAZ material fracture toughness properties. The ductile tearing resistance of clad metal acts as a first line of defense against cleavage fracture from small surface cracks embedded in the clad layer.

The curves that summarize the before and after irradiation K_{Jc} toughness versus temperature relations are given in Fig. 10. The solid and dashed lines for HAZ materials represent transition curves developed by compact specimen tests. Unfortunately, the HAZ-type compact specimens had to be irradiated in capsule space donated from another project and these were given three times the neutron dose of the clad beam specimens. For fitting the bend bar data in Fig. 10, the K_{Jc} curve for the HAZ material had been shifted down by 20°C (using ref. 18) to compensate for this excess exposure to produce the dashed line. The point illustrated by Fig. 10 is that the transition range toughness behavior of the bend bar specimens, representing the toughness of combined microstructures, is evidently dominated by the toughness characteristics of HAZ material. Also, the HAZ material had suffered a 10°C greater transition temperature shift than the base metal (not shown). Despite this, the base metal always had the lowest toughness so that the design conditions for both unirradiated and irradiation conditions were always conservatively represented by the toughness of the base metal.

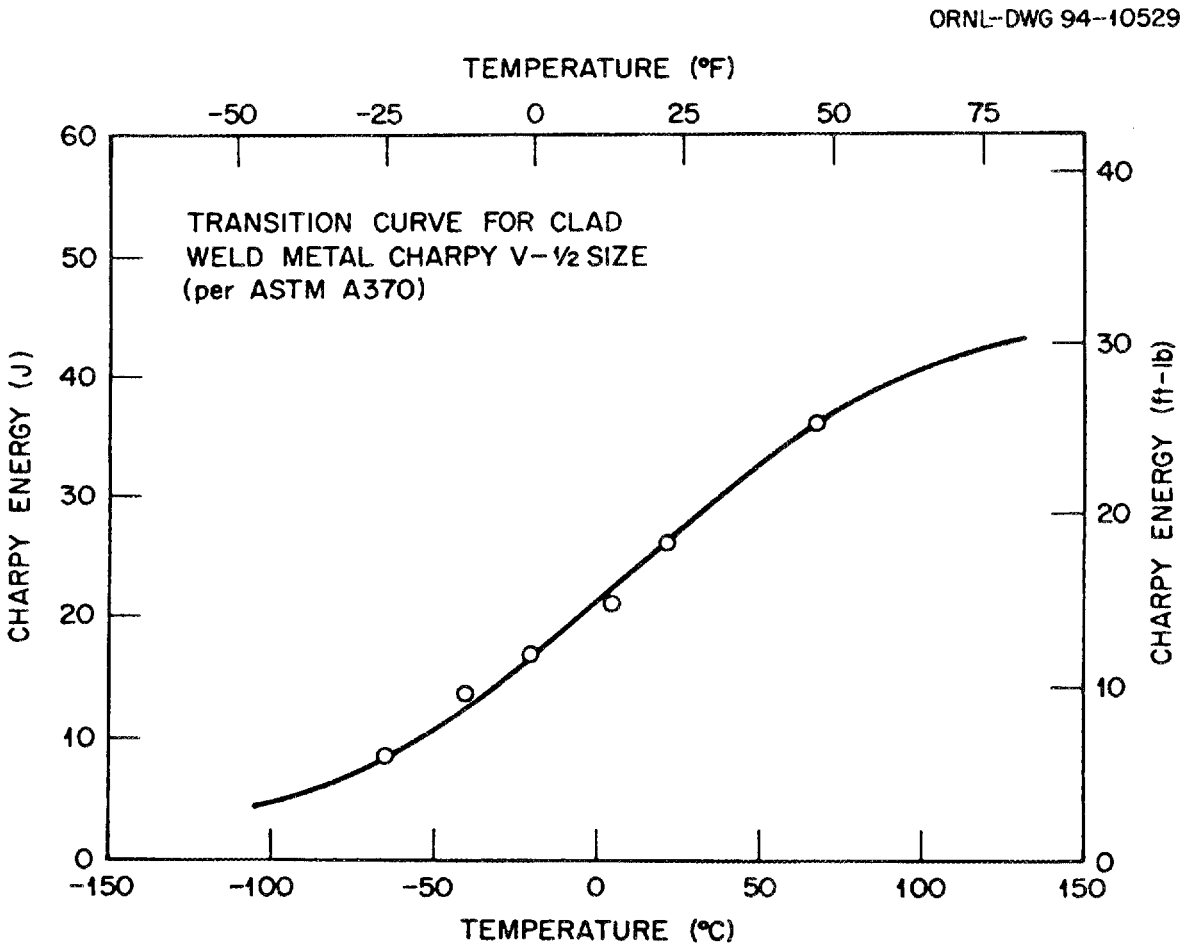

Fig. 7. Charpy transition curve of clad metal using 1/2 size Charpy specimens as defined by ASTM Standard Test Methods and Definitions for Mechanical Testing of Steel Products (A 370-92).

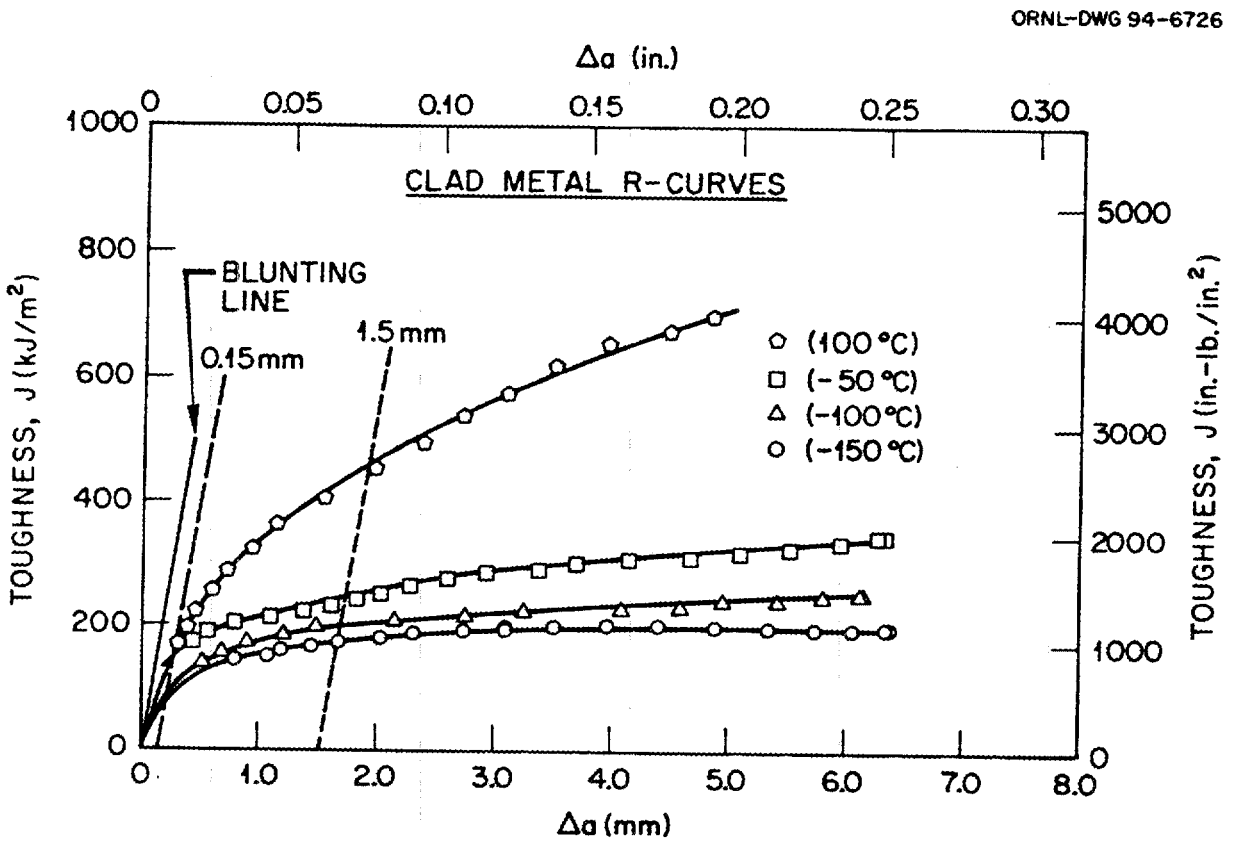

Fig. 8. J-R curves for clad metal shown to be highly test temperature dependent.

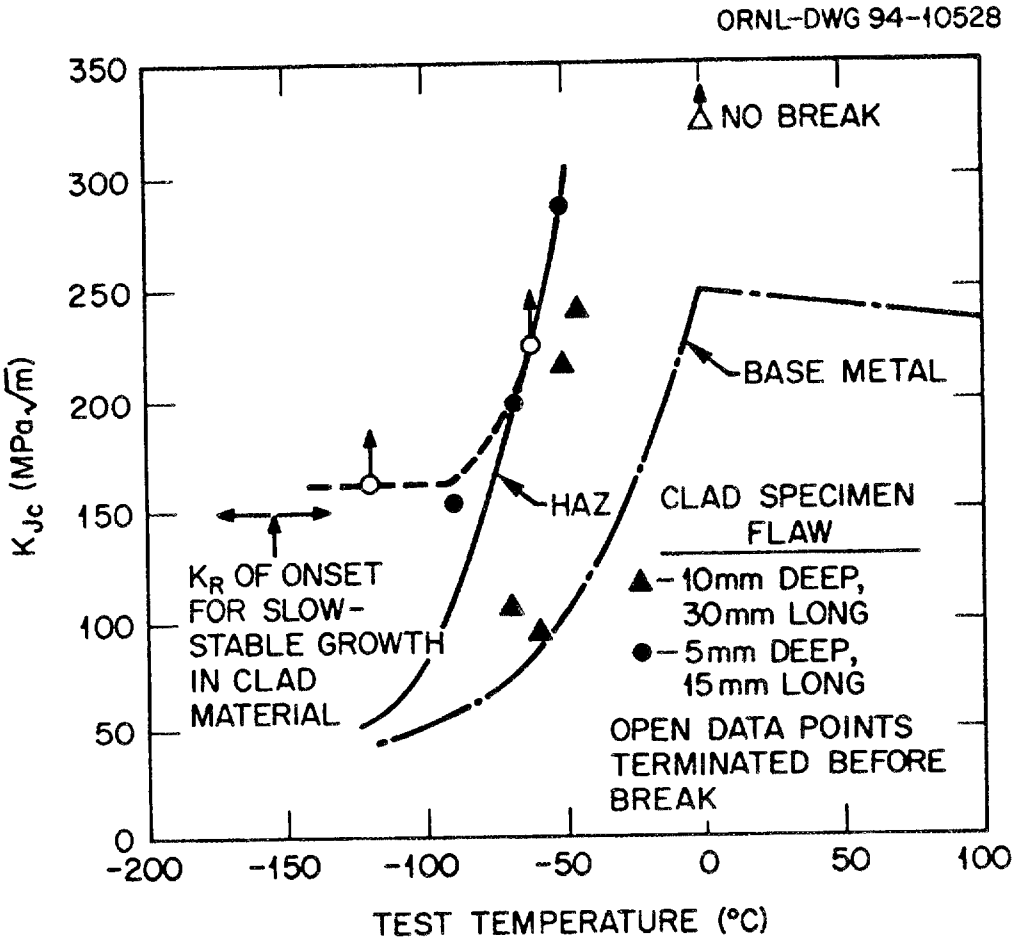

Fig. 9. Transition curves for HAZ and base metal (A 533 grade B) determined from compact specimens and data points from bend bar specimens with surface cracks.

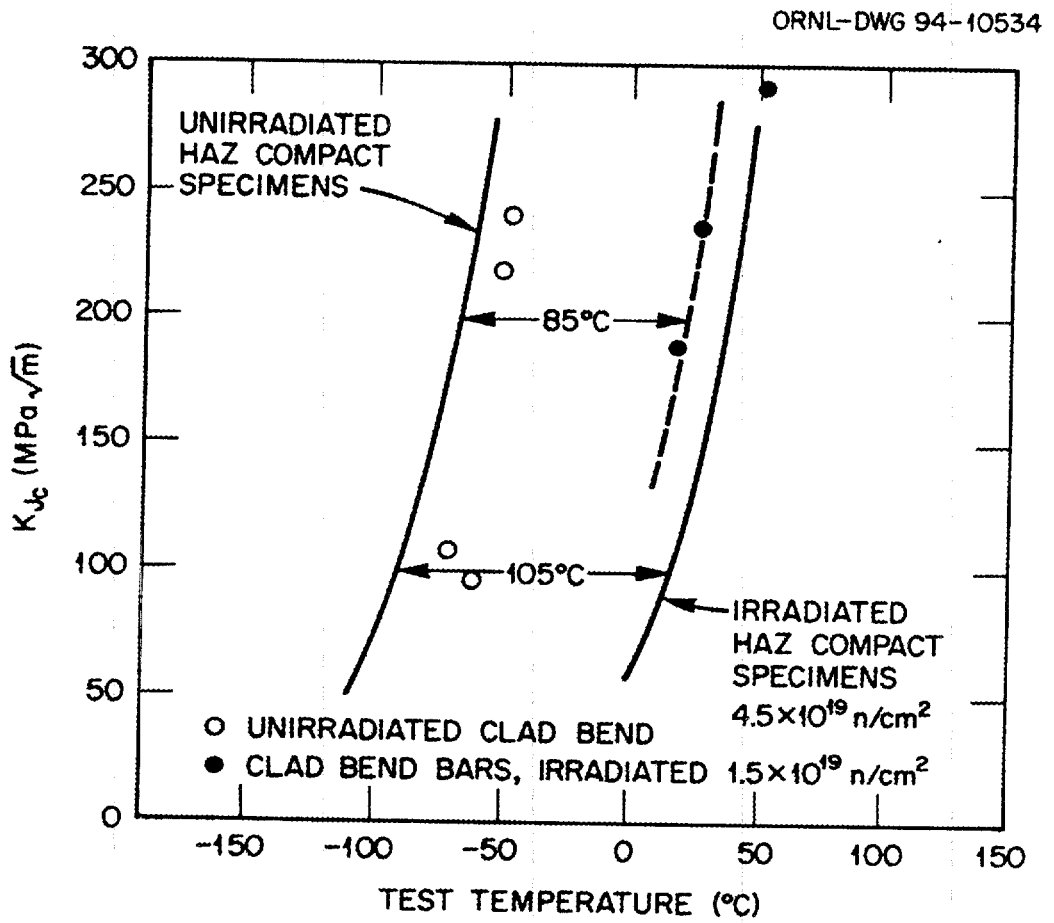

Fig. 10. Before-and-after irradiation K_{Jc} versus temperature curves for HAZ materials determined by compact specimens. Data points are for surface-cracked clad beams, before and after irradiation.

Other work at ORNL that contributed experimental evidence concerning the effects of cladding was the thermal shock experiments (TSE) of an intermediate size cylinder* with cladding on the inside (thermal shock) surface.[17] The purpose of these experiments, as it was with the previously discussed ORNL clad beam tests, was to prove that clad metal can restrict or retard the subclad propagation of cleavage cracks. The presumption is that as long as the clad remains intact, the high toughness clad layer would apply closure force across the clad metal to base metal interface, thereby reducing crack driving force stress intensity factor. The experimental results were expected to confirm analytical models developed on both subclad and through-clad flaws.

The cylinder base metal was A 508 class 2 steel, but, as with the work reported in ref. 15, the material was given an embrittling heat treatment that raised the RT_{NDT} temperature to 66°C (150°F) to simulate irradiation embrittlement. The interior wall was clad over three-fourths of its circumference with Inconel 600 and the remainder with type 304L stainless steel. After a two-layer strip weld clad application, the vessel received a 7-h stress-relief anneal at 620°C (1150°F). The stress-relief anneal time applied here is about one-third of the stress-relief anneal time applied in the production of commercial power production reactor vessels. In this case, the toughness of the HAZ layer under the cladding may not be better than that of the base metal. For four successive tests, various initial subclad flaws and subsequent surface flaws were positioned at the midlength of the cylinder. Transient thermal stresses were created by heating the cylinder to 93° (200°F) and with the exterior surface insulated, quenching the cylinder in a liquid nitrogen bath. Four thermal shock tests were conducted with the same cylinder (TSE-8 to TSE-11) with flaw geometries altered in shape and size between tests to explore different crack driving force conditions. Baseline performance information of an unclad intermediate cylinder of the same material was available from a previous experiment, TSE-7.[19] In that particular thermal shock experiment, a severe crack bifurcation pattern had developed from one central 37-mm-long by 19-mm-deep surface crack. The same flaw in the clad cylinder, TSE-9, given the same severity of thermal shock produced only crack pop-in with the flaw tunneling under the cladding about 6 mm. Clearly this was an experimental demonstration of a beneficial effect. However, the cylinder wall cooling rates were not equal between TSE-7 and TSE-9 because of the thermal conductivity protection from the clad metal in the latter case. Consequently, the base metal temperatures were higher and thermal stresses lower after specific units of time.

As mentioned, there were many flaws in a variety of shapes, sizes, and locations in the clad cylinder tests. Each crack initiation event was checked against the calculated crack driving force and these were compared to material fracture toughness, K_{Ic}. A

---

*Intermediate vessels are 991 mm outside diameter, 1220 mm long, and 152 mm wall thickness.

general pattern of underestimating the inelastic stretching of the cladding and thus overestimating the beneficial crack closure forces from the cladding was noted.[17] Hence, the net result of the clad cylinder tests was a successful demonstration that cladding tends to suppress crack initiation and subsequent crack propagation in base metal, but the benefit with respect to initiation was not as great as predicted by calculation.

DISCUSSION - CLADDING EFFECTS

The experimental evidence from the three references cited (refs. 15, 16, and 17) suggests that the cladding process does not adversely affect the transition temperature performance of the base metal. In one of the three cases, the clad welding operation was followed by a longer time of stress-relief anneal (16 h) , which enhanced the fracture toughness of the heat-affected zone. The HAZ did not benefit the crack-arrest toughness behavior in the ref. 17 experiments presumably because of less tempering time. The fact that the cladding process results in high tensile residual stresses in the cladding seems to be of secondary significance with respect to the behavior of small surface cracks and small subclad cracks. Clad layering without sufficient stress-relief anneal could very well lead to a different result, but this is not a likely scenario for commercial reactors.

The clad metal that typically contains 5 to 15% delta ferrite (a microstructure that is required to prevent hot cracking in the weld metal) does not have the good crack growth resistance of wrought austenitic stainless steels. Hence, the benefit of the crack closure force from the clad layer is smaller than expected. The most effective source of crack instability resistance is provided by the underlying heat-affected zone material. It is not clear that the presently used finite-element models have incorporated these experimentally demonstrated toughness characteristic. Hence, until such material interaction relationships are captured analytically, the continued use of the conservative analysis approach presently recommended in the ASME Code appears to be advisable.

WARM PRESTRESS

The warm prestress (WPS) phenomenon may offset other material degradation phenomena, such as irradiation and strain aging embrittlement, evidence of which is developed in experiments using test specimens that have had no loading history prior to testing. Warm prestress is a phenomenon describable in terms of the crack tip plastic zone developed at service load that effectively blunts the crack such that the component or vessel retains the capability of sustaining a load level previously held. The load-carrying capability is sustained even though the surrounding body of material can be shown to be in an embrittled condition.

The following information on warm prestress experiments supports the premise that the WPS phenomenon is reliably achieved in reactor vessel steels. Nevertheless, there are reasonably held doubts as to the reliability of WPS-derived toughness values because of uncertainties about the influence of damage mechanisms that can reduce the toughness of the material in the protective plastic zone.

There are two primary categories of WPS cycles.[20] In one case precracked specimens are WPS loaded at an upper shelf temperature at which the material cannot fail in cleavage. This can be followed by unloading and cooling to a lower temperature at which the specimen or component is then reloaded to failure (LUCF). The alternative case is to cool without unload to a test temperature in the cleavage range at which the loading is resumed until fracture occurs (LCF). In the latter case, the plastic zone is not partially compressed as it is with a full unload. Hence, the crack tip blunting from plastic deformation and the associated work-hardening are not partially undone through a Bausinger effect. In both cases, the loading to failure is done at a temperature at which the surrounding material is embrittled.

Early experiments did not provide strong evidence of warm prestress effects, primarily because of a conservative decision to satisfy plane strain constraint requirements during the warm preload step.[21] As a result, the warm prestress, K_I, was, by necessity, kept low and the instability values at fracture temperature, K_f, tended to fall within the K_{Ic} scatter band for virgin material, but with a high toughness bias. Thus, the experiment was only a weak demonstration of the warm prestress effect.

Later work by Stonesifer et al.[20] involved WPS experiments on A 533 grade B plate with much higher K_{WPS} loading. Compact specimens of 4T plan view size but with 50.8 mm thickness (2 in.) were used. In this case, the plan view size was sufficient to maintain dominant elastic conditions at K_{WPS} loads that were terminated at the point of onset of slow-stable crack growth. Plane-strain thickness requirements were ignored. Warm preload temperature was 177°C (350°F) and the K_{WPS} was 190 MPa$\sqrt{m}$ (175 ksi$\sqrt{in.}$). Both LUCF and LCF cycles were employed and each was replicated 10 times. Figures 11 and 12 show typical test records for such cycles. The method of calculating K_f is important. Even though the reloading test records are linear, credit is taken for prior plastic deformation in the calculation of K_f at fracture using plastic zone-adjusted crack size. In the case of LCF cycles, the failure load was always greater than the warm prestress load. Unless some form of prior plastic deformation credit is taken in the calculation of K_f for LCF or LUCF cycles, the potential paradoxical result could be that, between two specimens of virtually equal dimensions but loaded to different loads, the one that is more highly loaded but analyzed without considering past history generated plastic zone could have the lower crack driving force. The specimens given the LUCF cycle were unloaded and kept stored at room temperature for several weeks, allowing plenty of time for strain aging of the plastic zone. There was no clear evidence of a strain aging effect at room temperature. The LCF cycle had no significant delays between the WPS loading and

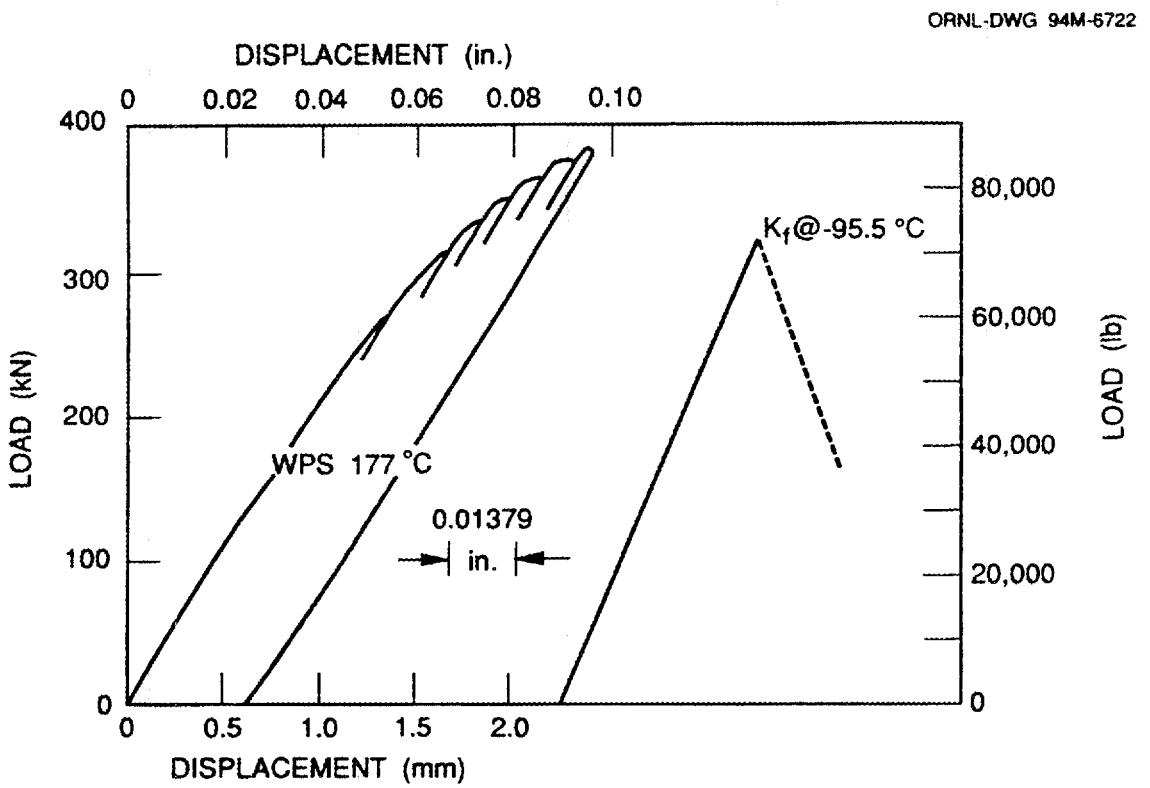

Fig. 11. Test records for LUCF loading, showing WPS loading at 177°C and K_f loading to fracture at −95.5°C.

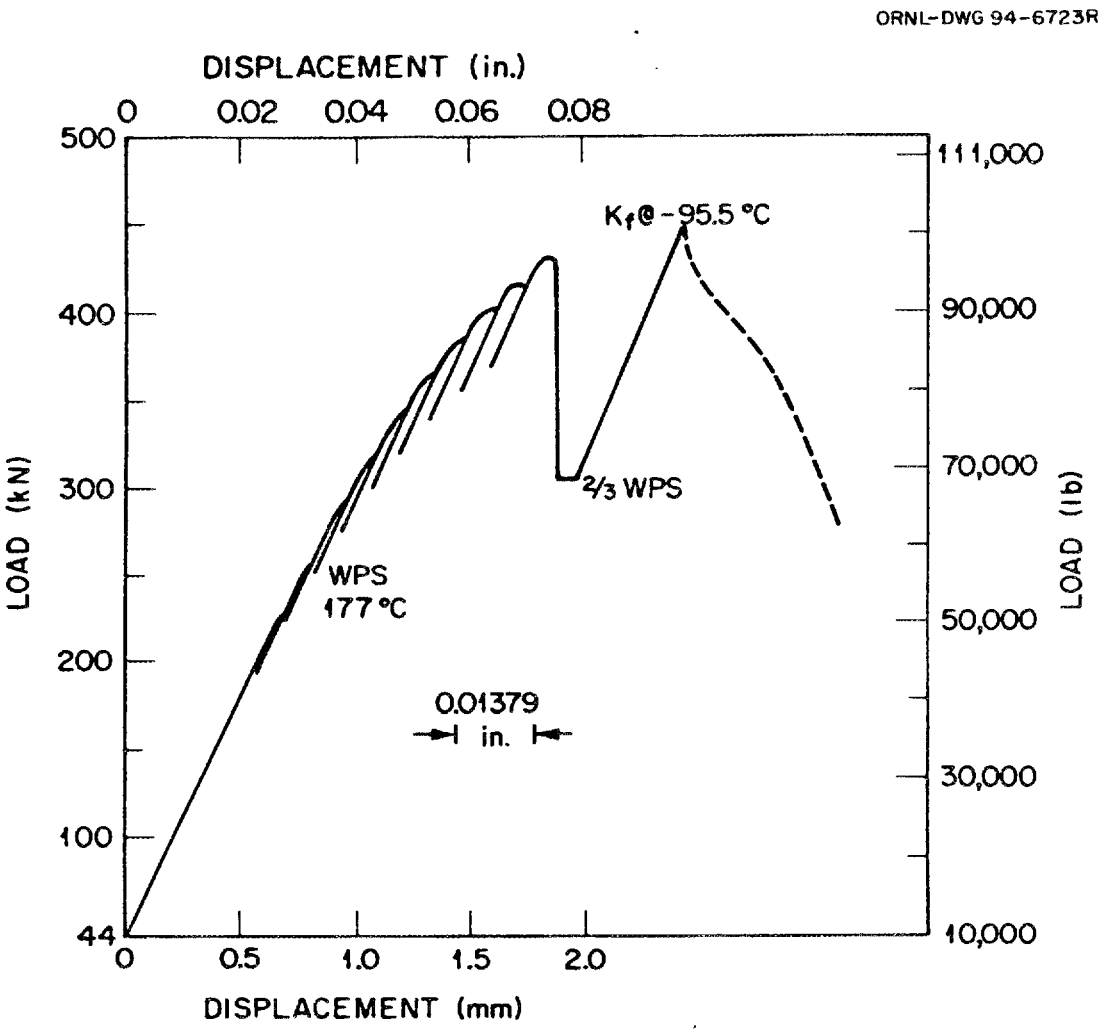

Fig. 12. Test records for LCF loading, showing WPS loading at 177°C, retained load at 2/3 P_{WPS}, and resumed loading to failure at K_f.

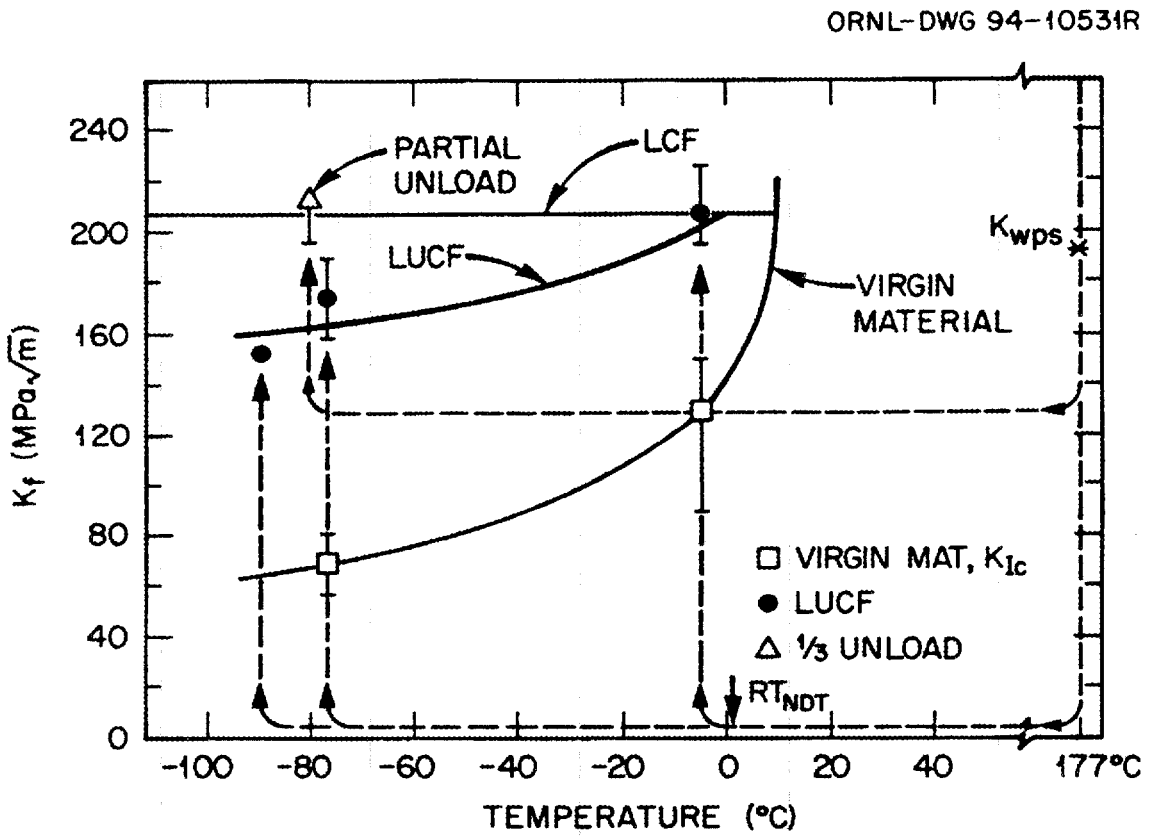

Fig. 13. Material transition curves for K at fracture (K_f) representing baseline toughness transition and transition behavior as altered by LUCF and LCF warm prestress cycles.

low temperature testing so that strain aging was not a consideration in any event. Figure 13 shows how the two types of WPS cycles affect the material fracture toughness versus temperature curve. The LCF cycles show 100% retention of the crack tip blunting effect of WPS loading. LUCF cycles show some reduction of the blunting effect caused by the complete unloading, but, nevertheless, a sizable benefit is retained.

A recent paper by Lidbury and Birkett[22] reported on investigations of the warm prestress effects on A 533 grade B steel for K_{WPS} loading up to K_{WPS} = 350 MPa$\sqrt{m}$. The experiments were somewhat similar to the work of Stonesifer et al.,[20] except that 0.8T compact specimens were used. This makes the analysis of elastic-plastic effects in the calculation of K_f in ref. 22 an especially important factor in the quantification of the WPS effect. In this case, credit for prior plastic deformation imparted during K_{WPS} loading was not credited in the calculation of K_f in the LUCF cycles. The WPS effect in LCF cycles was strong, with P_f/P_{WPS} (fracture load/WPS load) generally of the order of 1.10 ± 0.05. The LUCF cycles generally showed WPS benefits, but not of the order of the Stonesifer et al.[20] results, ostensibly due to the difference in the methods of calculating K_f.

One part of the Lidbury work involved the prestraining and aging of the material in bulk form prior to the making of WPS test specimens. The result was a transition temperature shift in the baseline fracture toughness transition curve. There was no particular damage done to the WPS characteristics of the material in subsequent WPS testing. Another auxiliary experiment reported in ref. 22 was to simultaneously strain age and warm prestress specimens by slowly loading them at an upper-shelf temperature of high strain aging propensity; 290°C (555°F). Other specimens were loaded rapidly to avoid strain aging. Both types were given LUCF and LCF cycles. The result was that WPS effects were not altered by strain aging in the LCF cycles. The authors observed, from their own work and from the work of others, that strain aging steel prior to WPS loading causes a baseline shift of transition temperature, but that the subsequent WPS phenomenon is apparently not altered. A more thorough study of crack tip damage mechanisms was recommended, however.

DISCUSSION - WARM PRESTRESS

Warm prestress experiments have suggested that there can be an existing safety margin that could be employed in failure assessment of aging reactors that is currently not being used. On the other hand, it is difficult to utilize the potential advantage gained from a phenomenon that is not completely understood. For one thing, there is no standard practice or commonly accepted elastic-plastic computational methodology by which the warm prestress characteristics of materials can be evaluated. In addition, the combined effects of irradiation, strain aging damage, or fatigue damage on the WPS characteristics of pressure vessel steels have not been thoroughly researched. On the other hand, the mechanism that causes the effect,

plus over 20 years of operation at 288°C (550°F) should significantly diminish strain aging potential in steels. The possibility that there might be accrued WPS safety margins for aged nuclear vessels is probably quite good. Experiments should be designed to define this potential by conclusively proving the nondeterioration of the WPS effect from metallurgical damage mechanisms.

TRANSITION TEMPERATURE TOUGHNESS

The strategy that is currently in use to define the transition temperature of reactor vessel steels is over two decades old. At the time of formulating this strategy, nondestructive examination capabilities and experience in applying fracture mechanics to structural steels were both limited. Despite this, the ASME Pressure Vessel Research Council (PVRC) task group, formed to develop a code practice, managed to devise a workable plan that melded what was known about fracture mechanics and empirical transition temperature methods to arrive at a means for the setting of safe allowable operating conditions. Conservative margins were used to compensate for the lack of having well-tested technical models. Now it is proposed to refine these margins. The replacement of the dynamic K_{IR} curve with something approaching the K_{Ic} curve in order to open the LTOP operating window has already been mentioned. Another way to open this window would be to sharpen the accuracy of transition temperature definition. For example, it is now possible to eliminate the use of RT_{NDT} from drop-weight and Charpy tests to position the lower-bound K_{Ic} curve and thus improve the accuracy of such curves. Currently there is one lower-bound K_{Ic} curve that subtends widely scattered K_{Ic} data, all of which were gathered from tests performed prior to 1980. The curve shape was assumed to be universally applicable to all pressure vessel steels of a given class and their weld metals. This curve is presently adjusted for irradiation effects by using Charpy V-notch data[23] or by calculating the transition temperature shift using the U.S. Nuclear Regulatory Commission *Regulatory Guide 1.99* (ref. 18).

Statistical methods are now available that can model data scatter and that define the median fracture toughness versus temperature for data distributions at one or (if preferred) a few test temperatures. In addition, it is now possible to employ weakest-link statistical theory to predict specimen size effects on the median fracture toughness and standard deviations of data distributions over a fairly wide range of specimen sizes and test temperatures. Hence, it is possible to use only fracture mechanics-based data to directly establish transition temperature shift. Specimens that are small enough to fit in surveillance capsules can be used to provide size-scaled fracture mechanics-type information.

A draft ASTM test practice is currently under development that defines the criteria for the development of qualified data, i.e., valid K_{Jc} values, and statistical methods are

used for the calculation of confidence limits on data scatter and safe margin adjustment.*

An example of the application of the procedure to a weld metal taken from the beltline of a commercial reactor vessel follows. The data distribution of six 4T compact specimens is fitted with a three-parameter Weibull function of the following form:

$$P_f = 1 - \exp\left\{ - \frac{(K_{Jc} - 20)}{(K_\theta - 20)} \right\}^4 . \tag{1}$$

The term P_f is the cumulative probability factor of equaling or exceeding a given value of K_{Jc} and K_θ is a scale parameter that quantifies the fracture toughness level of the data set. Figure 14 is a plot of K_{Jc} data using logarithmically normalized coordinates that linearize Eq. (1). The scale parameter value can be calculated based on K_θ, which is determined graphically as shown in Fig. 14.

Specimen size effects on K_{Jc} can be calculated using weakest-link statistical theory. The Weibull model above can be reduced to the following simple-to-use expression:

$$K_{(med)x} = 20 + \{K_{Jc(med)} - 20\} \left(\frac{B_o}{B_x}\right)^{1/4} . \tag{2}$$

Material tested in specimens of thickness B_o that show a median fracture toughness $K_{Jc(med)}$ will have a median $K_{(med)x}$ when tested in specimens of thickness B_x. Equation (2) can be used to convert data from specimens of a variety of sizes to values corresponding to one size. It has been proposed that such data, when converted to correspond to 1T compact specimen size, will fit a universal transition temperature curve, termed a master curve.[24] Median fracture toughness for 1T specimens is well modeled by the equation:

$$K_{Jc(med)} = 30 + 70 \exp\{0.019(T - T_o)\} . \tag{3}$$

---

*Draft 6, "Test Practice (Method) for Fracture Toughness in the Transition Range," ASTM Task Group E08.08.03, April 1994.

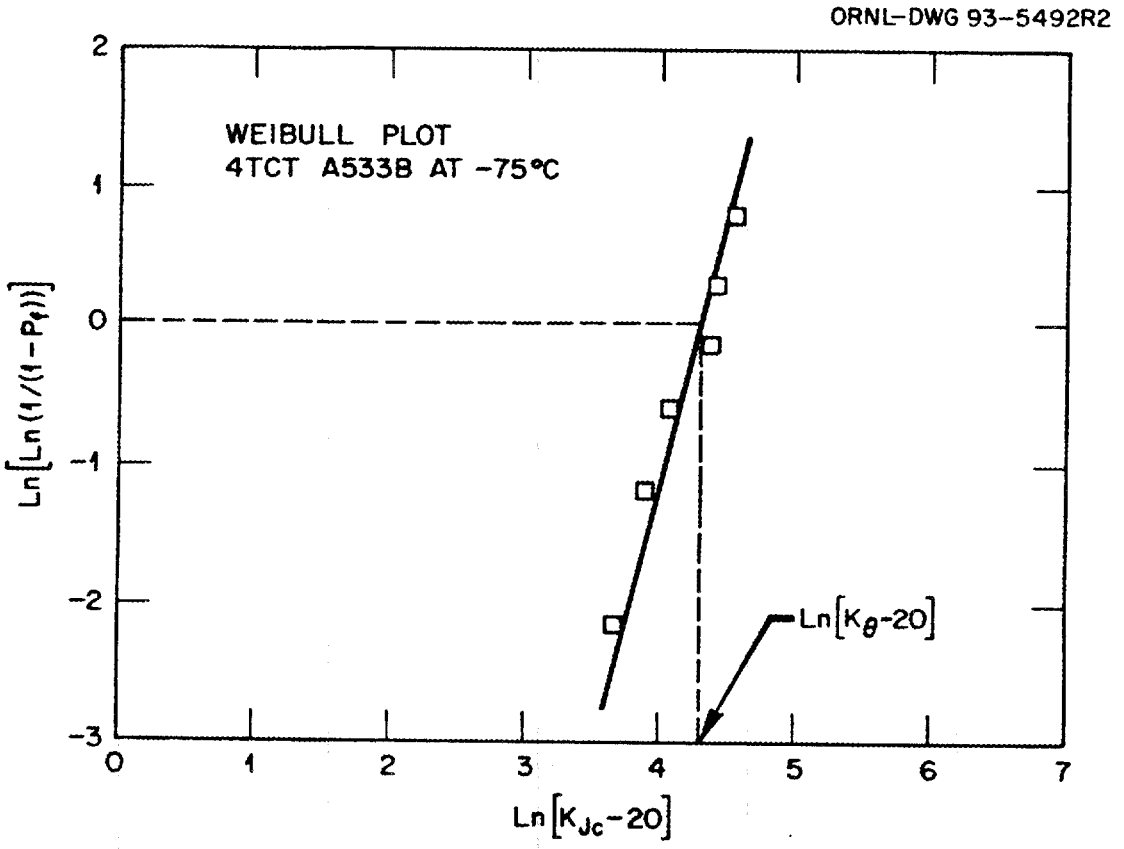

Fig. 14. Weibull three-parameter fit [Eq. (1)] of K_{Jc} data from 4T specimens of A 533 grade B steel at −75°C.

The temperature, T_o, is a reference temperature at which the median fracture toughness, K_{Jc}, of 1T specimens is 100 MPa$\sqrt{m}$ (see Fig. 15). Because the toughness data are known to almost always fit a Weibull distribution of the form of Eq. (1), the standard deviation of such data is automatically defined. The following equation applies:

$$\sigma = 0.28 \left[\frac{K_{Jc(med)} - 20}{K_{Jc(med)}} \right] . \qquad (4)$$

The factor, 0.28, is derived from the Weibull slope of four. Standard deviation is a function of the position in the transition range. It is a simple matter to look up standard normal deviates so that upper and lower confidence levels can be computed. Figure 16 shows the lower curve for 5% cumulative probability applied to the 1TCT data set shown.

Further details on the procedure can be obtained in the ASTM proposed test practice. The master curve fit to the Electric Power Research Institute (EPRI) K_{Ic} data that had been used to establish the K_{Ic} lower bound is shown in Fig. 17. Note by comparing the ASME lower-bound K_{Ic} curve to the 5% cumulative probability curve that the ASME K_{Ic} curve has no consistent statistical probability definition.

DISCUSSION - TRANSITION TEMPERATURE TOUGHNESS

The introduction of statistical methods into transition temperature work has provided a capability for dealing with the enormous data scatter usually associated with transition range data. Data scatter can be mathematically modeled and, with the augmentation of weakest-link theory, specimen size effects on fracture toughness can also be modeled. It is becoming possible to characterize transition range toughness without having to resort to large test programs with dozens of specimens in a variety of sizes. The latter approach was used to establish the ASME lower-bound K_{Ic} curve. Since it is now possible to adjust K_{Jc} toughness values for specimen size, it is also possible to establish a master curve that is developed on the bases of one specimen size. The 1T size was chosen. The master curve represents a fit to median values of 1T fracture toughness data distributions. It is a universal curve that characterizes a large class of pressure vessel steels and their weld metals. The potential that slow-bend Charpy bar testing could have to establish the reference temperature, T_o, of the master curve is currently being evaluated. This concept of one universal curve is not new, since the lower-bound K_{Ic} curve has been used for more than 20 years as an RT_{NDT}-adjustable curve of universal shape. The master curve position is set on the abscissa using a reference temperature established from fracture mechanics-type tests. Fewer specimens and specimens of a size compatible with surveillance capsule space limitations can be used to establish the master curve and associated confidence

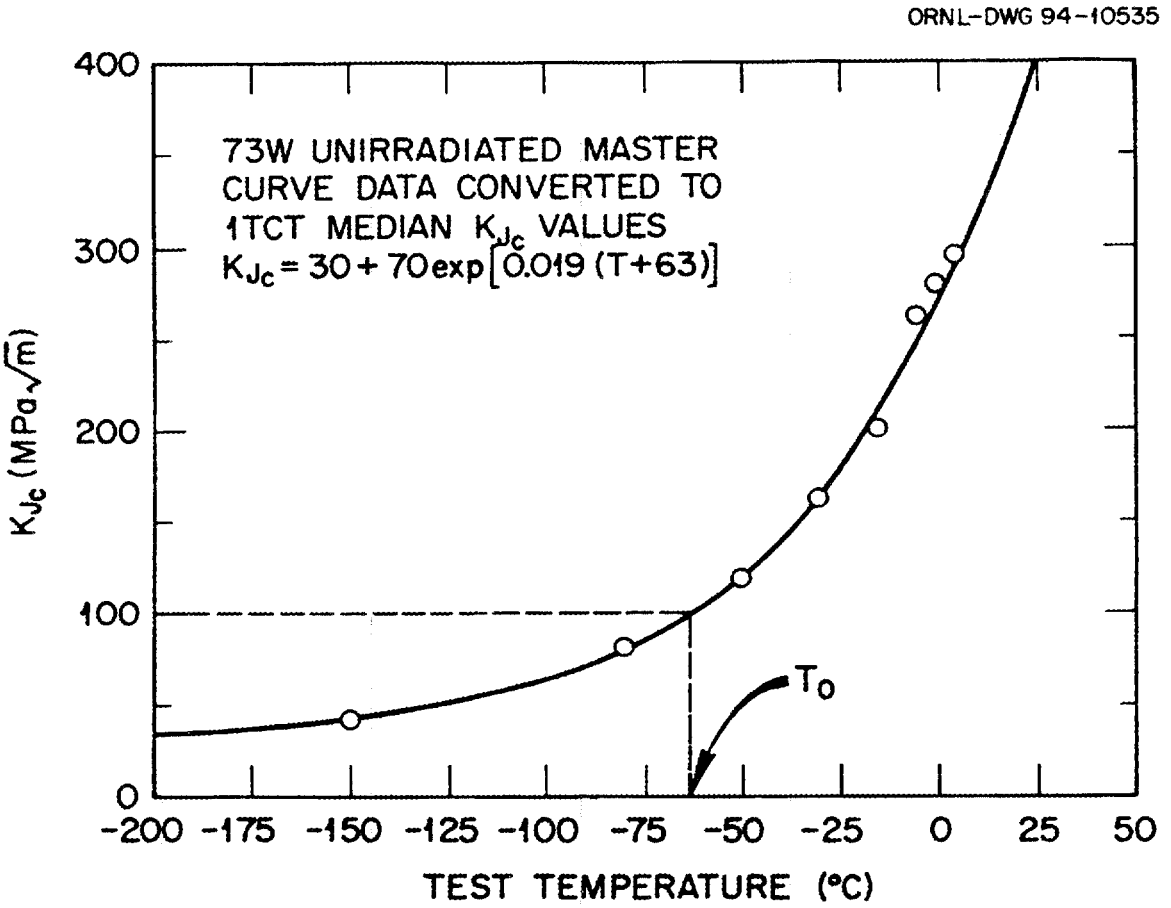

Fig. 15. Example master curve from the HSSI Fifth Irradiation Series showing the median value of K_{Jc} for a 1T compact specimen versus test temperature.

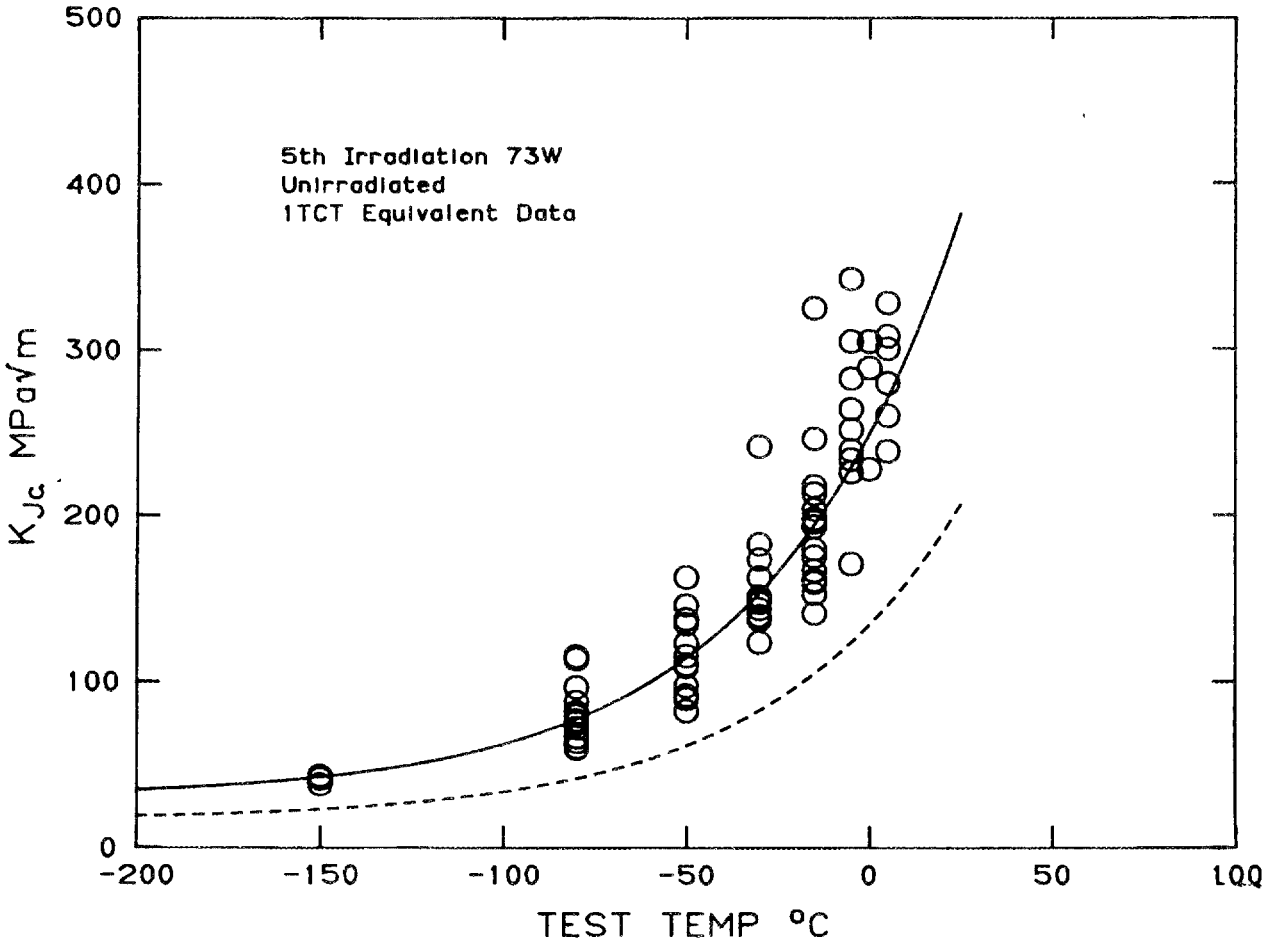

Fig. 16. Master curve for HSSI Fifth Irradiation Series data for weld 73W. Data points are for individual measured toughness values converted to 1T equivalent values. Dashed curve is 5% cumulative probability line (i.e., 95% of data are expected to be above the line).

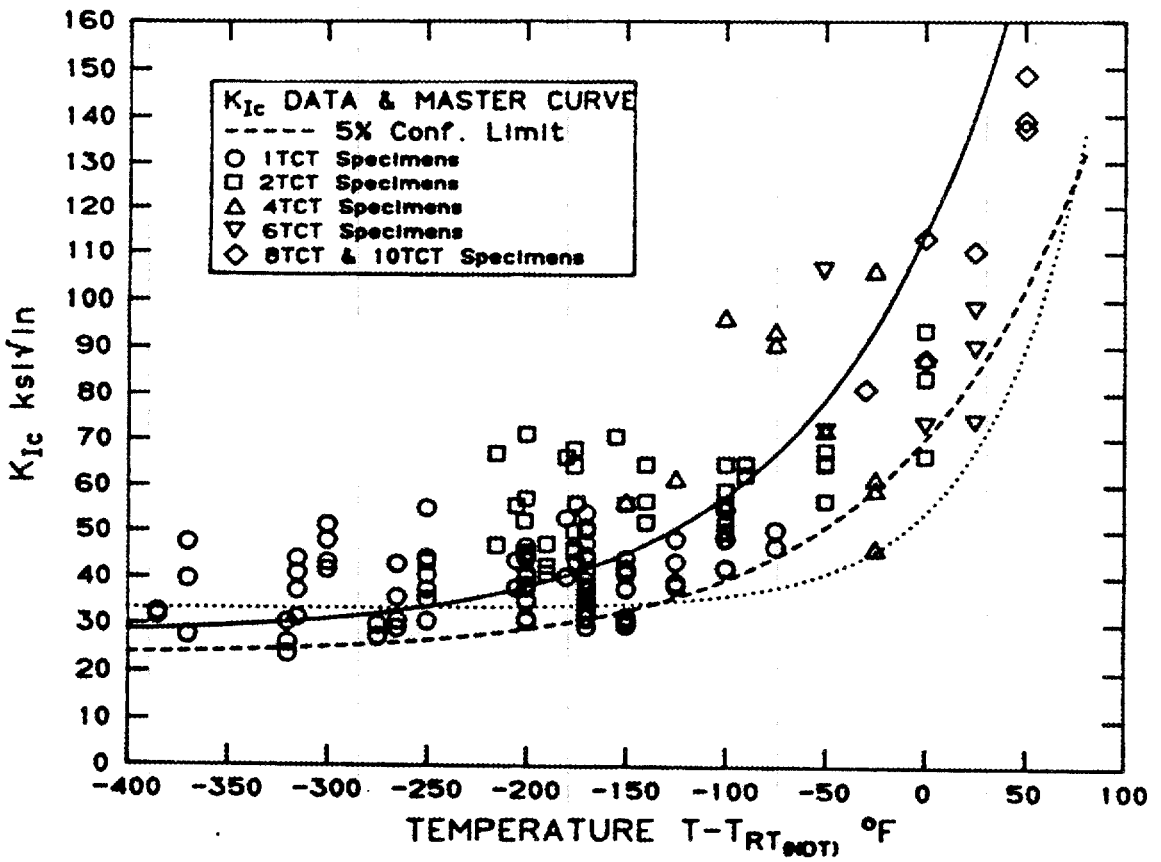

Fig. 17. Master curve developed for ASME K_{Ic} data showing 5% confidence limit and ASME Code lower-bound (dotted) curve. Data points are not size corrected.

limits. The need for correlations between K_{Ic} values and empirical transition temperature estimation by Charpy V-notch (CVN) or drop-weight (NDT) temperature is thereby eliminated.

STRAIN RATE EFFECTS

Strain rate effects are covered in the ASME Code by using the extremes of the lower-bound K_{Ic} curve for quasi-static loading and the lower-bound K_{IR} curve for dynamic loading rates and crack arrest.[25] These curves are separated by 35°C (63°F) at the 100-MPa√m (91-ksi√in.) fracture toughness level (Fig. 18). The aforementioned 35°C represents the potential enlargement in the LTOP operating window width, obtainable by replacing the K_{IR} curve with the K_{Ic} curve.

The objective of a recent study under the Heavy-Section Steel Technology (HSST) Program was to revisit the data used to establish both curves and to determine if there is any cause to make some adjustments. This work is partially complete and one letter report of the two planned reports has been issued. The first report[26] dealt with K_{Ic} data and it had two interesting findings. One was that all the K_{Ic} values determined at test temperatures below $T - RT_{NDT} = -106°C$ (−160°F) were not considered when establishing the lower-bound K_{Ic} curve shown in Fig. 18. When all of the available data down to −195°C (−320°F) were subsequently added, it was determined that true lower-bound on K_{Ic} is 26.4 MPa√m (24 ksi√in.), not the 36.5-MPa√m (33.2-ksi√in.) lower-bound value implied by the EPRI equation.[27] The other finding was that the K_{Ic} curve in the ASME Code, Section XI, Appendix A, was not the same as that of the widely used EPRI equation shown in Fig. 18. The ASME Code prior to 1992 contained the solid line curve shown in Fig. 19. However, the difference was small. Recent data added from the HSST Fifth Irradiation Series were not lower-bounded by the ASME Code curve, but were lower-bounded by the EPRI equation (Fig. 19). The ASME Code has recently been revised, reducing at most by ~4.5°C, the previously mentioned temperature difference between the static K_{Ic} curve and the dynamic K_{IR} curve.

The K_{Ia} and K_{Id} data used to establish the K_{IR} curve are also being reviewed. In this case it appears that the representation of the lower-bound K_{IR} toughness is conservative (Fig. 20). However, note that the K_{Ia} crack-arrest data almost exclusively establish the position of the lower-bound curve. Again, the data from the HSSI Series tests[28] in the form of crack-arrest data have been compared to the Code curve data. There were two A 533 grade B weld metals, 72W and 73W, in the unirradiated and irradiated conditions (Fig. 21). A total of 112 specimens were tested in accordance with ASTM Standard Method E 1221 in this case. The data significantly disagree (23°C) with the ASME lower-bound K_{IR} curve position relative to the RT_{NDT} temperature.

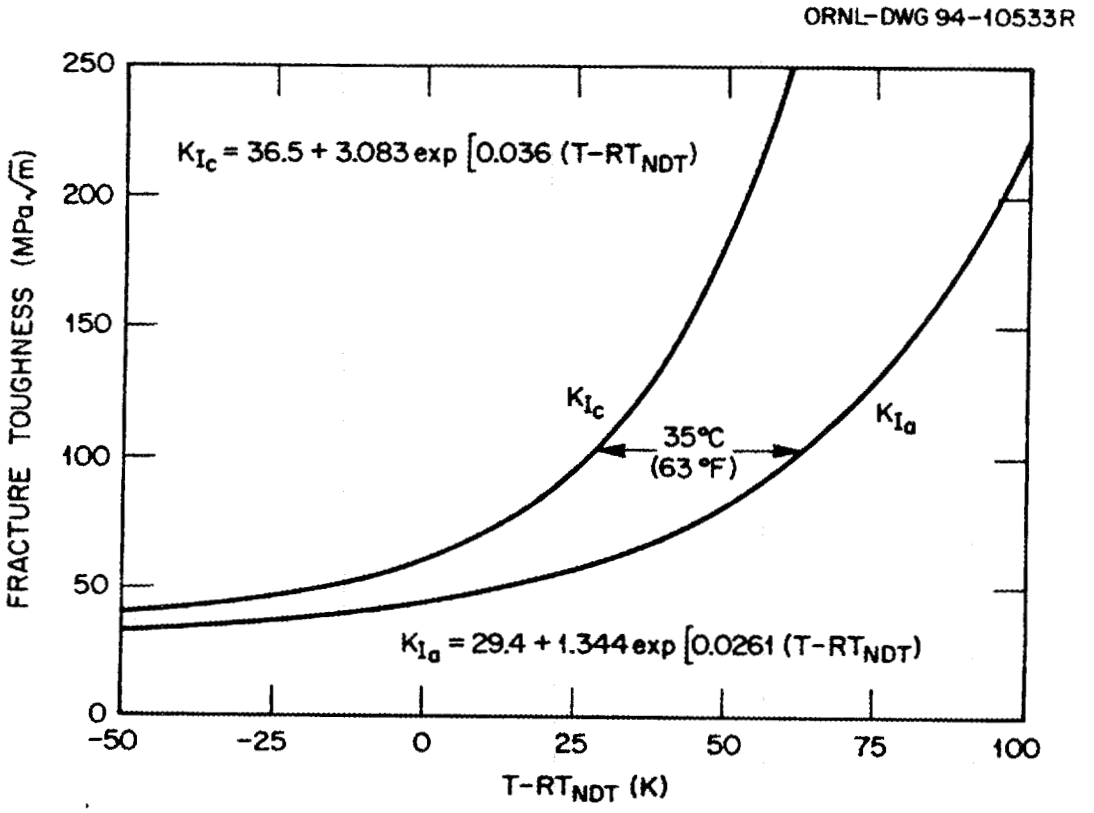

Fig. 18. ASME Code K_{Ic} and K_{Ia} curves from Section XI, Appendix A, 1992.

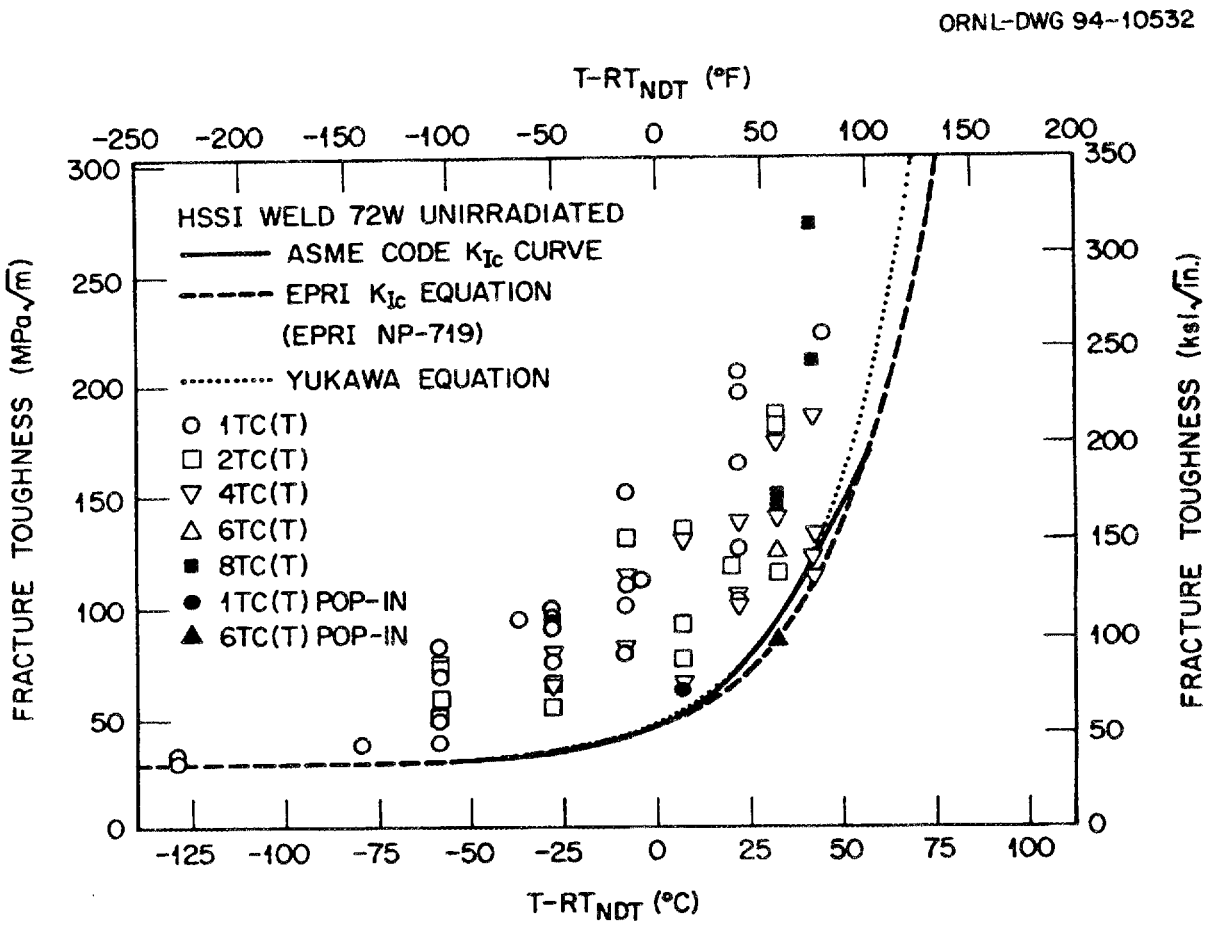

Fig. 19. EPRI static initiation fracture toughness data base from ref. 25 (open points) compared with HSSI Fifth Irradiation Series data (closed points). Curves are ASME prior to 1993 (solid curve), modified curve-fit equation from Yukawa (dotted curve), and the EPRI equation for K_{Ic} lower-bound (dashed curve).

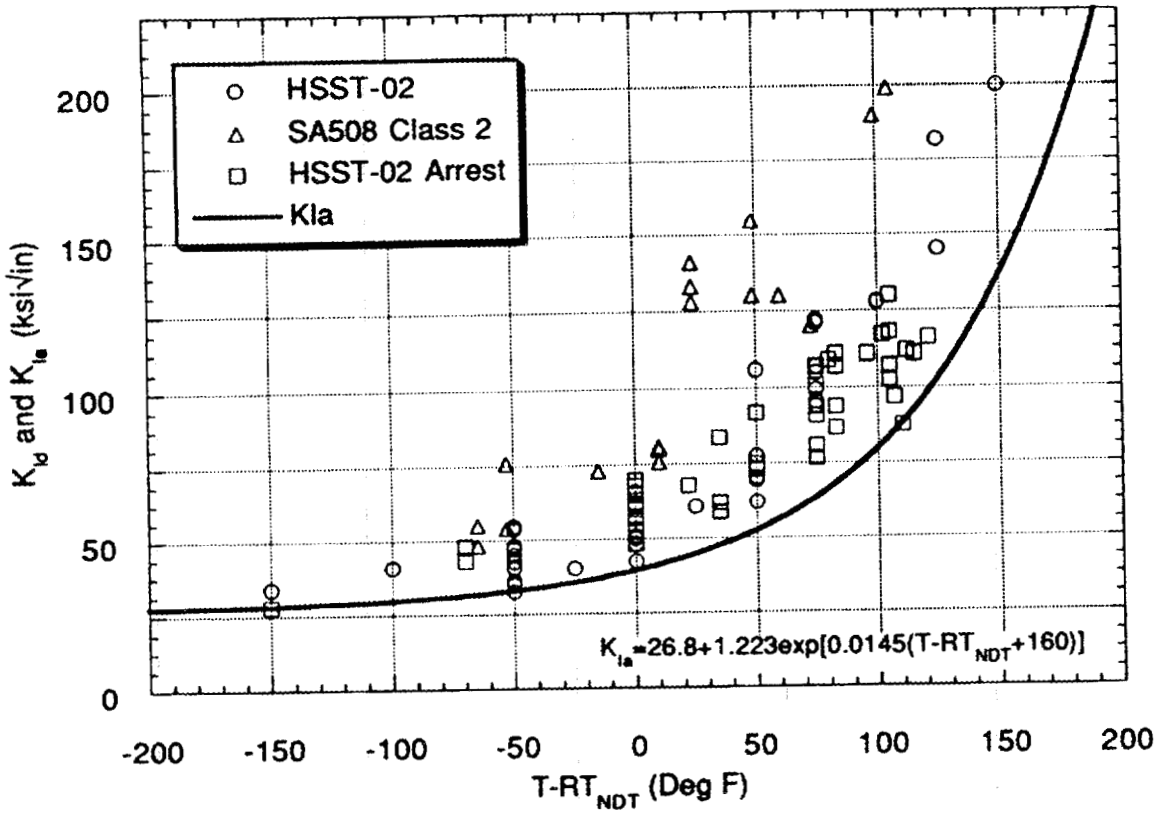

Fig. 20. EPRI K_{Id} and K_{Ia} data base and the EPRI lower-bound curve fit to the data.

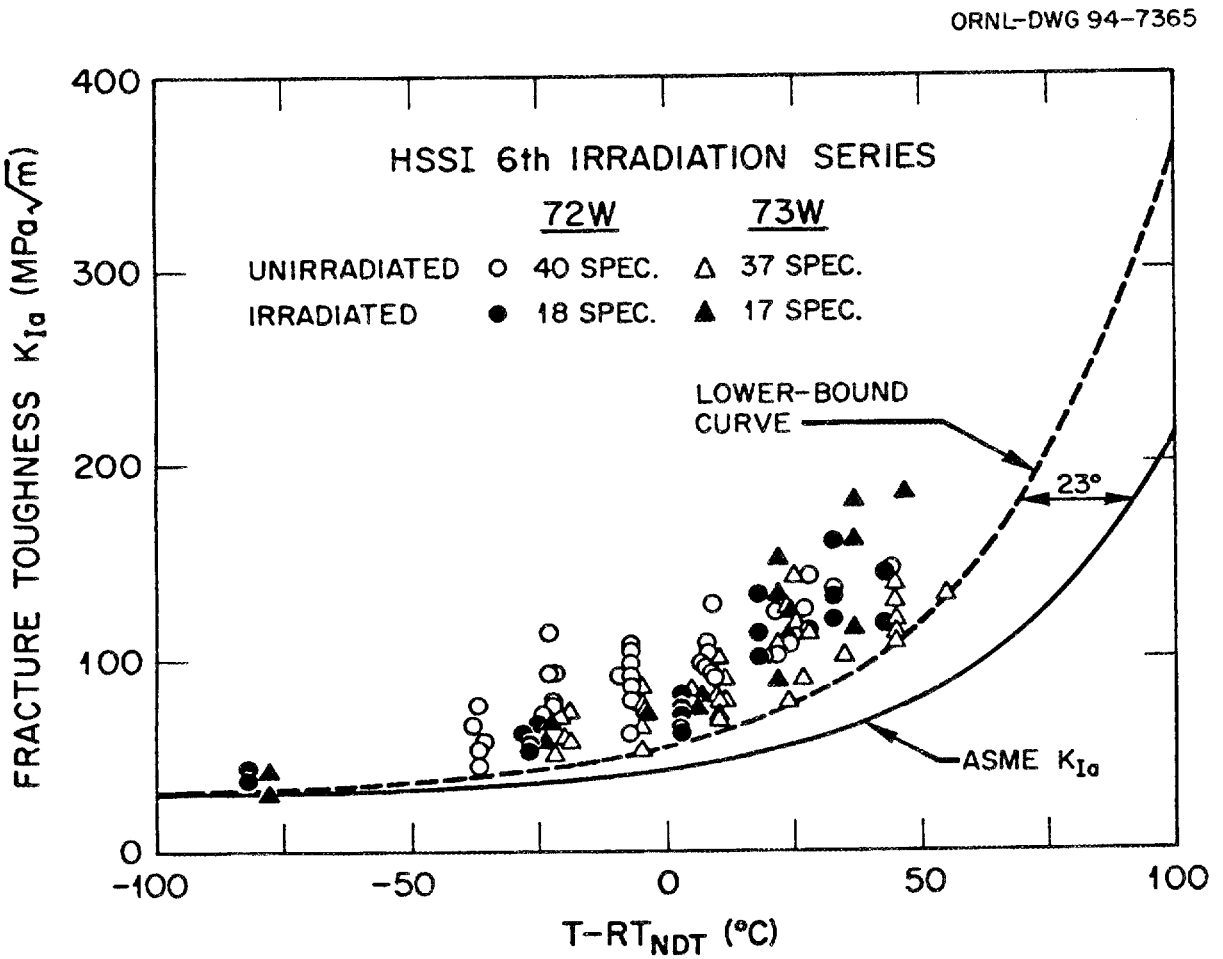

Fig. 21. HSSI Fifth Irradiation Series K_{Ia} test data compared with the ASME Code K_{IR} (K_{Ia}) curve.

Another set of data available in the literature comes from a cooperative program sponsored by the Japan Atomic Energy Research Institute.[29] The purpose of this program was to develop a second set of data to define the lower-bound K_{Ic} and K_{Ia} curves for Japanese steels. The materials were A 533 grade B and A 508 base metal and weld metal. These results were reported in 1986. The crack-arrest toughness values for base and weld metals, referenced to $T - RT_{NDT}$ are shown in Figs. 22 and 23, respectively. The dashed lines shown were not used in ref. 29, but are added here to demonstrate the similarity of the outcome to the HSSI tests reported in ref. 28. The disagreement of the lower-bound fit and RT_{NDT} adjusted K_{IR} curve is evident. The offset is 20°C in one case and 30°C in the other. In these cases, the crack-arrest values were, for the most part, valid by E 1221, whereas the original ASME data predated an ASTM consensus test standard. The important conclusion here is that these results suggest that the temperature separation between static and dynamic toughness curves for pressure vessel steels is about two-thirds of that implied from the EPRI K_{Ic} and K_{IR} lower-bound toughness curve equations.

ASTM guidelines for designing a surveillance program are covered in Standard E 185-82 (ref. 23). Currently the transition temperature shift due to irradiation damage is measured in terms of the Charpy 41-J (30-ft-lb) shift. This toughness value had been selected on the assumption that this point on the Charpy energy curve approximately corresponds to the drop-weight NDT temperature. Both test practices are empirical in nature and both involve dynamic loading. It now appears that these dynamic methods may give a different ΔRT_{NDT} transition temperature shift than static tests. For one example, the International Atomic Energy Agency (IAEA) has compared dynamic versus static Charpy and compact specimen transition temperature shifts on two pressure vessel steels.[30] After irradiation of A 533 grade B steel at 1.2×10^{19} neutrons/cm^2, ΔRT_{NDT} calculated from dynamic Charpy data at 41 J was 118°C, whereas the value of ΔRT_{NDT} calculated from static Charpy three-point bend data was 155°C. A similar result was found using compact specimens of A 508 steel, but these data were too preliminary to be published.*

A serious shortcoming of a Charpy transition curve is that the true data scatter characteristic of a given material is seldom apparent. In particular, a random Charpy specimen selection process to determine a Charpy transition curve could result in a transition temperature anywhere within a 60°C scatter band. To illustrate, Fig. 24 resulted from generating Charpy data on a reactor beltline weld with A 508 base plates for specimen locations at five through-thickness positions and four evenly spaced locations around the girth.[31] Figure 24 represents the accumulation of data

---

*Technical discussions, K. Wallin, Technical Research Center of Finland, Espoo, Finland, and D. E. McCabe, Oak Ridge National Laboratory, Oak Ridge, Tennessee, September 10-11, 1992.

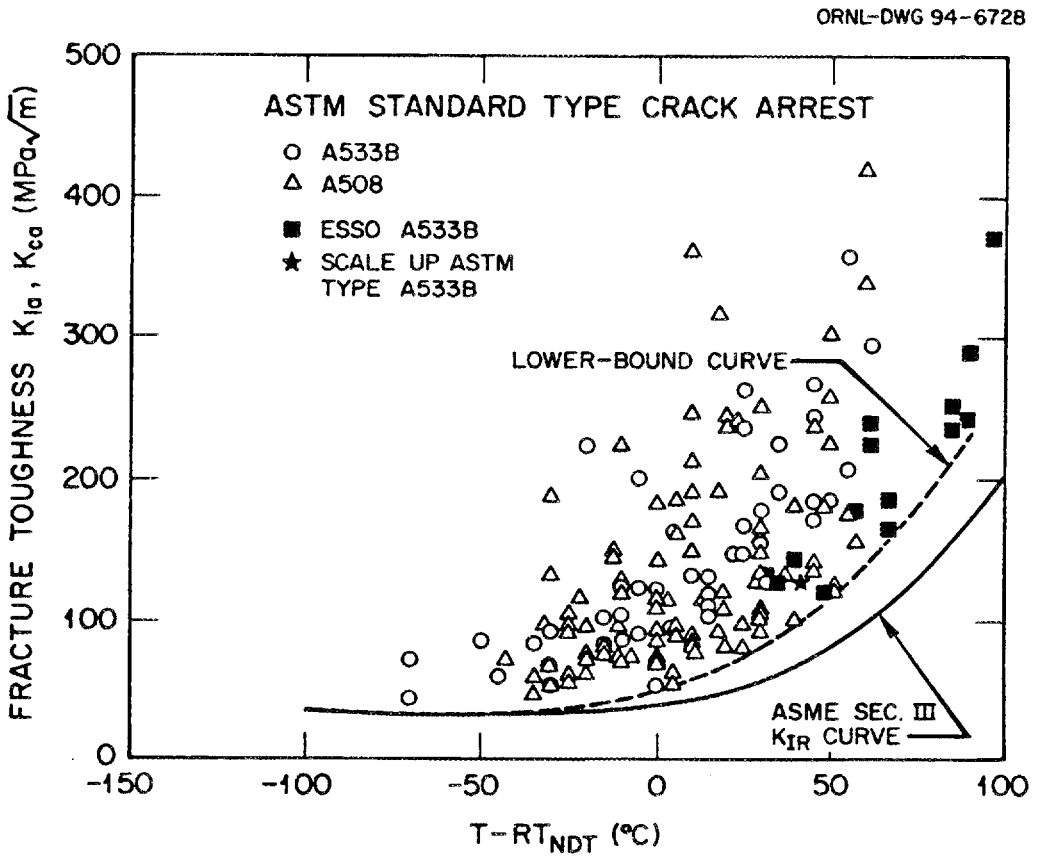

Fig. 22. Base metal crack-arrest toughness data from the Japanese (JAERI) round-robin tests, reproduced from ref. 27, with dashed line lower-bound fit added to show lack of agreement with ASME Code.

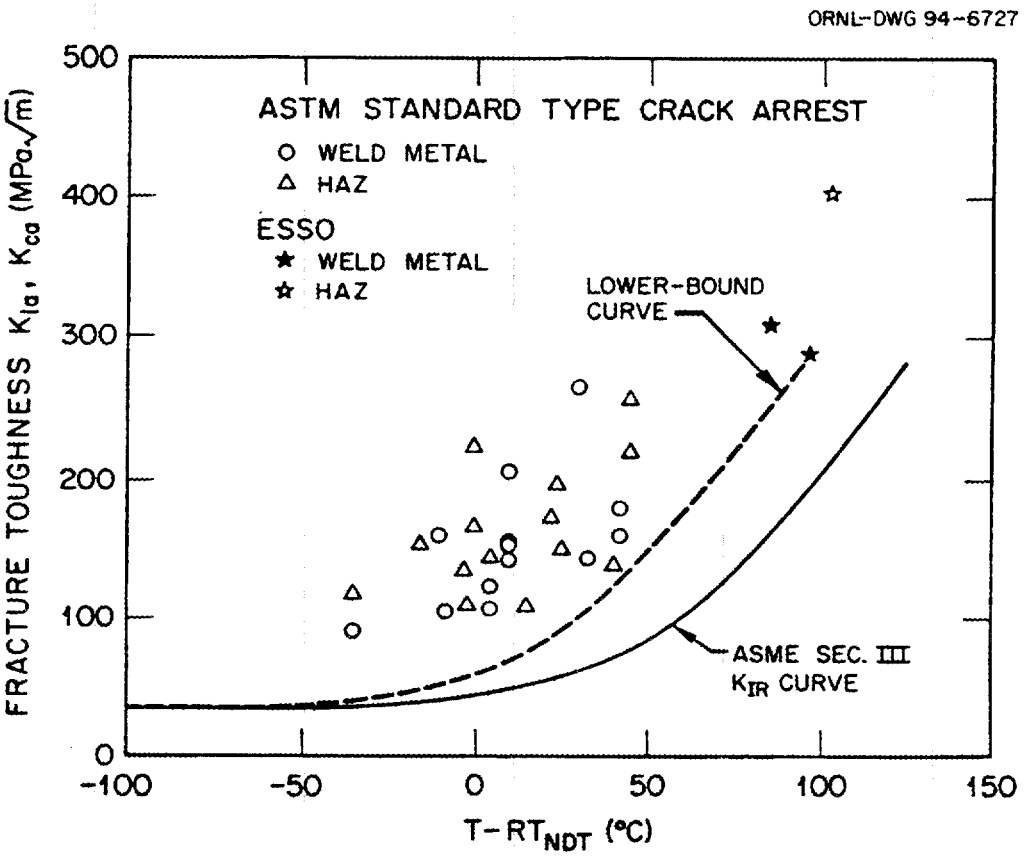

Fig. 23. Weld metal crack-arrest toughness data from the Japanese (JAERI) round-robin tests, reproduced from ref. 27, with dashed line lower-bound fit added to shown lack of agreement with ASME Code.

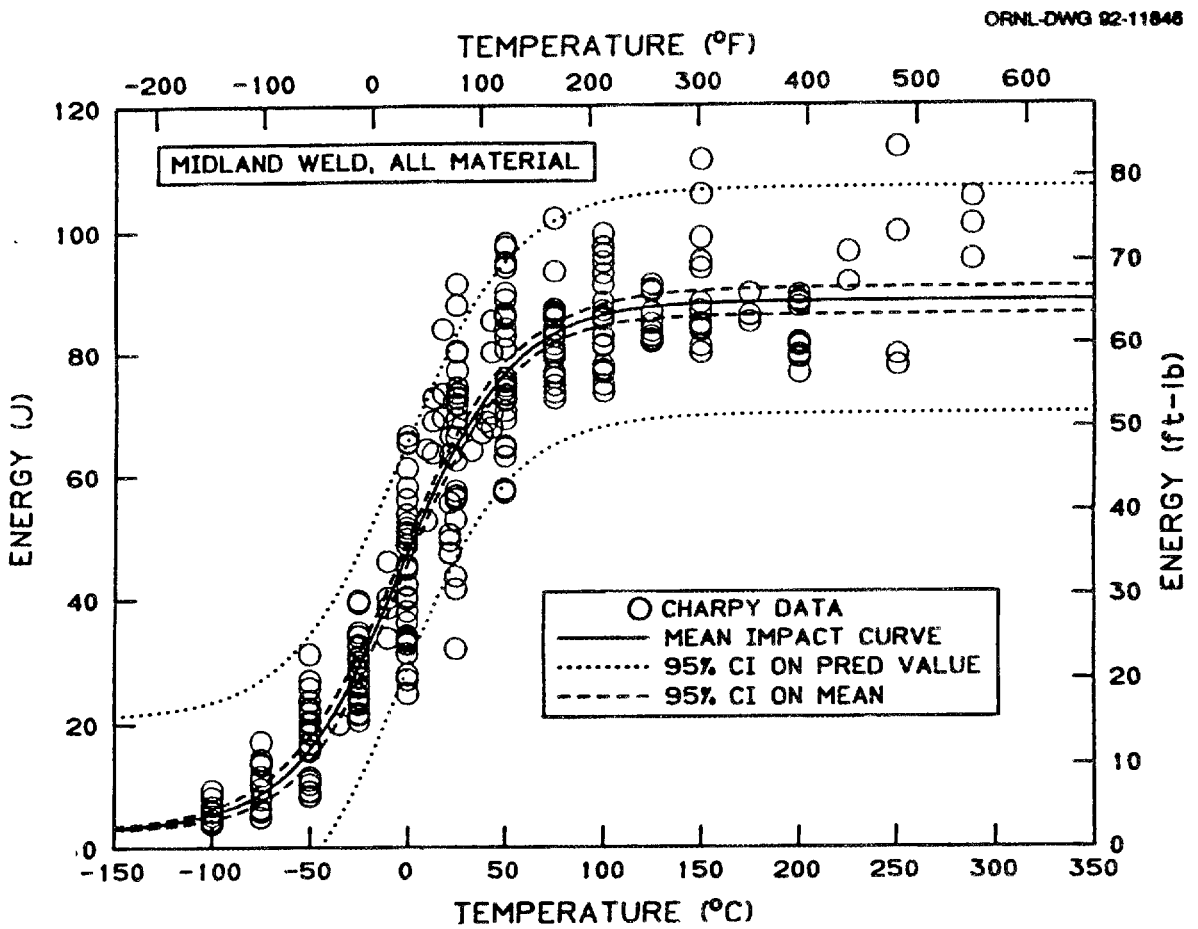

Fig. 24. Charpy V-notch impact energy versus test temperature for all specimens tested in the HSSI Tenth Irradiation Series. The solid curve represents the mean hyperbolic tangent curve fit and the dotted curves show the upper and lower 95% confidence limits with respect to the predicted CVN energy at any temperature.

from 19 Charpy transition curves for 19 selected locations of one weld material. Because this was a low upper-shelf weld metal, RT_{NDT} was determined from Charpy data. The lowest RT_{NDT} from these data was −20°C (−3°F) and the highest RT_{NDT} was 37°C (99°F). Since before-and-after irradiation 41-J (30-ft-lb) temperature differences are used to determine ΔTT, the potential for error can be as large as 60°C. This lack of accuracy is disturbing, considering that such data can be used as a basis for deciding the suitability of reactor vessel steels for continued operation.

DISCUSSION - STRAIN RATE EFFECTS

The K_{IR} curve and the recommended procedure for positioning the curve using drop-weight NDT temperature appears to be conservative. Recent K_{Ia} data developed with E 1221 valid tests suggest that the conservatism over static K_{Ic} amounts to about 20 to 25°C. More data are being generated in cooperative test programs currently in progress. These results will probably suggest that the vessel materials are not as strain rate-sensitive as the 1970s vintage K_{Ia} data had indicated. The use of the Charpy 41-J toughness value at which to quantify the transition temperature shift, ΔTT, due to irradiation damage appears to be an unsuitably inaccurate estimate that can be nonconservative for static ΔTT shift. Material variability is not well accounted for in the currently applied CVN transition temperature methodology.

Clearly, a better perspective on strain rate effects is needed. There is a need for more direct dynamic material toughness evaluations that can improve upon or replace the empirical test methods, and that are adaptable to surveillance capsule space availability. Consideration of data scatter (material variability) and the appropriate modeling of the same should be an integral part of the evaluation process.

SUMMARY

This letter report presents the results of various fracture toughness experiments in subjects that have been identified as relevant to the setting of safe pressure/temperature margins for low-temperature overpressurization protection (LTOP) transients. One proposal made is to replace the dynamic lower-bound K_{IR} curve with the static lower-bound K_{Ic} curve. In this matter, it is necessary to argue that there is no possibility of running cleavage cracks being initiated from small cracks that are located in or near regions of embrittled material. Other needs are to demonstrate that recent developments in transition temperature testing have improved the accuracy of placement of transition temperature curves. Also of interest is determination of the role of warm prestress effects for protection against onset of cleavage fracture in embrittled steels.

Brittle weld metal, brittle heat-affected zone (HAZ), and the HAZ subcategory of local brittle zones have been raised as subjects for evaluation as the possible sources of running cleavage cracks. All of the above are created by mistakes made in welding

practices and most of these mistakes can be alleviated by effective postweld heat treatment. Postweld heat treatment is standard practice in the fabrication of nuclear pressure vessels, so it is not too surprising that there have been no documented cases of reactor vessel failures from brittle zones of weldments. Evaluation of fabrication records and other data from research work on typical pressure vessel welds should be reviewed by engineers having expertise in this area before the existence of a problem is declared.

Experiments that model the various configurations of small cracks in the region of cladding have indicated that such cracks are not damaging to the structural performance of reactor vessels. Surface cracks in clad metal must propagate stably under increased load to the HAZ material in order to trigger cleavage in HAZ material. The crack growth resistance of clad metal is the so-called first line of defense against cleavage. A properly performed stress-relief anneal after the cladding process can produce an underclad HAZ of superior fracture toughness compared to that of the base metal. Consequently, the rules of analysis given in the ASME Code appear to be suitably conservative.

Problems with excessive data scatter and specimen size effects have prevented the use of fracture mechanics tests to directly establish transition temperature for plant-specific analyses. Statistical methods have been developed that now make it possible to use fracture mechanics test practices on surveillance capsule size specimens to establish transition temperature for full-thickness sections. This should eliminate the uncertainties that come from the use of correlations with Charpy V-notch and drop-weight nil-ductility transition tests. Current research is being conducted to determine if precracked Charpy V-notch specimens loaded in slow bend can be used with the new technology. With the statistical approach, it is possible to establish accurate confidence limits on fracture toughness data scatter that in turn can be used to collapse margins of safety to more reasonable levels.

Experiments that have been made to demonstrate warm prestress effects have clearly shown the strong potential available in nuclear pressure vessel steels. The phenomenon raises the lower-shelf toughness of the transition temperature curve, the extent of which depends on the warm prestress (WPS) load and the conditions of unloading after the warm prestress cycle. The methodology applied to test record analysis after the prior WPS cycle is debatable and deserves more consideration. Another issue is how metallurgical damage mechanisms such as strain aging or subsequent fatigue loading influence the effectiveness of the WPS phenomenon. The experimental evidence developed to date has indicated that metallurgical damage mechanisms have no influence. However, more experiments and careful consideration of all possible information sources are needed before the advantage of WPS can be justified for LTOP control.

The advantage of replacing the K_{IR} curve with the K_{Ic} lower-bound curve to characterize the material fracture toughness part of the LTOP boundary is about 35°C (65°F) at the 100-MPa√m fracture toughness level. The accuracy of this spread depends on the accuracy of dynamic K_{Ic} tests and crack-arrest K_{Ia} values developed prior to the existence of ASTM test standards. Recently developed data from two investigations have suggested that the 35°C spread might be about 10°C (18°F) too high (overconservative).

Currently, transition temperature shift due to irradiation damage, ΔTT, is measured by Charpy V-notch transition curve shift at the 41-J level or by predictions of the same using material chemical composition and fluence measurements. Recent work has shown that ΔTT from fracture mechanics tests can be significantly larger than that of the Charpy test. This appears to be an appreciable effect that potentially could cancel the advantages that are seen in margin relaxation justified from unirradiated static versus dynamic effects.

ACKNOWLEDGMENTS

The author would like to thank S. K. Iskander and J. G. Merkle for their technical review, helpful discussions, and comments. The preparation of this letter report was handled by J. L. Bishop.

REFERENCES

1. ASME Section XI Task Group on Reactor Vessel Integrity Requirements, *White Paper on Reactor Vessel Integrity Requirements for Level A & B Conditions*, EPRI TR-100251, Electric Power Research Institute, Palo Alto, Calif., January 1993.

2. J. G. Merkle, Martin Marietta Energy Systems, Inc., Oak Ridge Natl. Lab., *An Overview of the Low-Upper-Shelf Toughness Safety Margin Issue*, USNRC Report NUREG/CR-5552 (ORNL/TM-11314), August 1990.

3. R. T. Cheverton, J. W. Bryson, D. J. Alexander, and T. Slot, Martin Marietta Energy Systems, Inc., Oak Ridge Natl. Lab., *Pressure Vessel Fracture Studies Pertaining to the PWR Thermal Shock Issue: Experiments TSE 5, TSE 5A, and TSE 6*, USNRC Report NUREG/CR-4249 (ORNL-6163), June 1985.

4. W. F. Brown, Jr., *Ed., Review of Developments in Plane Strain Fracture Toughness Testing*, ASTM STP 463, American Society for Testing and Materials, Philadelphia, September 1970.

5. ASTM Special Committee on Fracture Testing of High Strength Metallic Materials, "The Slow Growth and Rapid Propagation of Cracks," *Materials Research and Standards*, 1(3), 389-93 (May 1961).

6. A. Barnes, "Local Brittle Zones in C-Mn Steel Multipass Welds," *Welding Institute Bulletin*, 94-98 (September/October 1990).

7. D. P. Fairchild, "Fracture Toughness Testing of Weld Heat-Affected Zones in Structural Steel," pp. 117-41 in *Fatigue and Fracture Testing of Weldments, ASTM STP 1058*, American Society for Testing and Materials, Philadelphia, 1990.

8. R. R. Irving, "A Hot Topic for Cold Steels (Researchers Air Views During Arctic Engineering Meeting in Houston)," *Metalworking News* (March 21, 1988).

9. J. A. Begley and T. R. Mager, *A Review of the Design Basis of the K_{IR} Fracture Toughness Curve*, EPRI TR-102852, Electric Power Research Institute, Palo Alto, Calif., August 1993.

10. R. Weck, "Brittle Fracture of a Thick Walled Pressure Vessel," *British Welding Research Association Bull.* (June 1966).

11. R. K. Nanstad, D. E. McCabe, B. H. Menke, S. K. Iskander, and F. M. Haggag, Martin Marietta Energy Systems, Inc., Oak Ridge Natl. Lab., *Irradiation Effects on Fracture Toughness of Two High-Copper Submerged-Arc Welds, HSSI Series 5*, USNRC Report NUREG/CR-5913, Vol. 1 (ORNL/TM-12156/VI), October 1992.

12. M. F. Kanninen and G. G. Chell, *An Assessment of the Importance of Vessel Cladding and Flaw Shape in the Analysis of Nuclear Reactor Pressure Vessel Integrity: A Report on an Experts Workshop Meeting*, SCIT:GC003, Electric Power Research Institute, Palo Alto, Calif., 1994.

13. R. D. Wiley, "Weld Deposited Cladding of Pressure Vessels," *British Welding Journal* 12, 378-93 (August 1965).

14. *ASME Boiler and Pressure Vessel Code. An American National Standard*, Sect. XI, Div. 1, IWB-3610, "Acceptance Criteria for Ferritic Steel Components of 4 in. and Greater Thicknesses," American Society of Mechanical Engineers, New York, 1992.

15. S. K. Iskander, G. C. Robinson, W. R. Corwin, B. C. Oland, D. J. Alexander, and K. V. Cook, Martin Marietta Energy Systems, Inc., Oak Ridge Natl. Lab., *Experimental Results of Tests to Investigate Flaw Behavior of Mechanically Loaded Stainless Steel Clad Plates,* USNRC Report NUREG/CR-5785 (ORNL/TM-11950), April 1992.

16. D. E. McCabe, "Fracture Resistance of Irradiated Stainless Steel Clad Vessels," pp. 348-60 in *Effects of Radiation on Materials: 14th International Symposium (Volume II) ASTM STP 1046,* American Society for Testing and Materials, Philadelphia, 1990.

17. R. D. Cheverton, J. W. Bryson, D. J. Alexander, and T. Slot, "Thermal Shock Experiments with Flawed Clad Cylinders," *Nuclear Engineering and Design,* 124, 109-19 (1990).

18. U.S. Nuclear Regulatory Commission, *Regulatory Guide 1.99, Revision 2,* "Radiation Embrittlement of Reactor Vessel Materials," May 1988.

19. R. D. Cheverton, S. K. Iskander, and D. G. Ball, "Review of Pressurized Water Reactor-Related Thermal Shock Status," pp. 752-66 in *Fracture Mechanics: Nineteenth Symposium, ASTM STP 969,* American Society for Testing and Materials, Philadelphia, 1988.

20. R. B. Stonesifer, E. F. Rybicki, and D. E. McCabe, Materials Engineering Associates, *Warm Prestress Modeling: Comparison of Models and Experimental Results,* USNRC Report NUREG/CR-5208 (MEA-2305), April 1989.

21. F. J. Loss, R. A. Gray, Jr., and J. R. Hawthorne, *Investigation of Warm Prestress for the Case of Small Delta-T During a Reactor Loss of Coolant Accident,* U.S. Naval Research Laboratory Report NRL-8198, March 9, 1978.

22. D. Lidbury and P. Birkett, "Effects of Warm Prestressing on the Transition Toughness Behavior of an A533B Grade B Class 1 Pressure Vessel Steel," pp. 264-85 in *Fracture Mechanics: Twenty-First Symposium, ASTM STP 1074,* American Society for Testing and Materials, Philadelphia, 1990.

23. *Standard Practice for Conducting Surveillance Tests for Light-Water Cooled Nuclear Power Reactor Vessels,* ASTM E 185-82, Vol. 03.01, American Society for Testing and Materials, Philadelphia, 1992.

24. K. Wallin, "Validity of Small Specimen Fracture Toughness Estimates Neglecting Constraint Corrections," in *Constraint Effects in Fracture: Theory and Applications, ASTM STP 1244,* American Society for Testing and Materials, Philadelphia, 1994.

25. *ASME Boiler and Pressure Vessel Code. An American National Standard*, Sect. XI, Div. 1, Article A-4000, "Materials Properties," American Society of Mechanical Engineers, New York, 1992.

26. R. K. Nanstad, J. A. Walker, and D. E. McCabe, *Preliminary Review of the Bases for the K_{ic} Curve in the ASME Code*, Letter Report, ORNL/NRC 93/15, July 1993.

27. ASME Section XI Task Group on Flaw Evaluation, *Flaw Evaluation Procedures: ASME Section XI*, EPRI NP 719-SR, Electric Power Research Institute, Palo Alto, Calif., August 1978.

28. S. K. Iskander, W. R. Corwin, and R. K. Nanstad, Martin Marietta Energy Systems, Inc., Oak Ridge Natl. Lab., *Results of Crack-Arrest Tests on Two Irradiated High-Copper Welds*, USNRC Report NUREG/CR-5584 (ORNL/TM-11575), December 1990.

29. Y. Sakai, K. Miya, I. Takahashi, and Y. Ando, "Properties of Heavy Section Steel Plates and Forgings for Nuclear Vessels Produced In Japan," *International Journal of Pressure Vessels and Piping*, **22**(2), 79-109 (1986).

30. RATU, *Nuclear Power Plant Structural Safety Research Program, Interim Report 1990-1991*, Para. 5.2, Finland's Energy Research Programs, Reviews B:120, Ministry of Trade and Industry Energy Department, Helsinki, Finland, 1992.

31. R. K. Nanstad, D. E. McCabe, R. L. Swain, and M. K. Miller, Martin Marietta Energy Systems, Inc., Oak Ridge Natl. Lab., *Chemical Composition and RT_{NDT} Determinations for Midland Weld WF-70*, USNRC Report NUREG/CR-5914 (ORNL/TM-6740), December 1992.

INTERNAL DISTRIBUTION

1. D. J. Alexander
2. B. R. Bass
3. J. W. Bryson
4. R. D. Cheverton
5. J. M. Corum
6. W. R. Corwin
7. D. F. Craig
8. T. L. Dickson
9. R. G. Gilliland
10. F. M. Haggag
11. H. W. Hayden, Jr.
12. S. K. Iskander
13. J. E. Jones Jr.
14. J. A. Keeney
15. W. J. McAfee

16-20. D. E. McCabe
21. J. G. Merkle
22. R. K. Nanstad
23. C. B. Oland
24. W. E. Pennell
25. C. E. Pugh
26. M. C. Rao
27. R. E. Stoller
28. ORNL Patent Section
29. Central Research Library
30. Document Reference Section
32. M&C Records Office
32-33. Laboratory Records
34. Laboratory Records - RC

EXTERNAL DISTRIBUTION

35. E. M. Hackett, Office of Nuclear Regulatory Research, MS T10-E10, NRC, Washington, DC 20555
36. A. L. Hiser, Office of Nuclear Regulatory Research, MS T10-E10, NRC, Washington, DC 20555
37. S. N. M. Malik, Office of Nuclear Regulatory Research, MS T10-E10, NRC, Washington, DC 20555
38. M. E. Mayfield, Office of Nuclear Regulatory Research, MS T10-E10, NRC, Washington, DC 20555
39. C. Z. Serpan, Office of Nuclear Regulatory Research, MS T10-E10, NRC, Washington, DC 20555
40. A. Taboada, Office of Nuclear Regulatory Research, MS T10-E10, NRC, Washington, DC 20555
41. K. R. Wichman, Office of Nuclear Reactor Regulation, NRC, Washington, DC 20555
42. W. H. Bamford, Westinghouse R & D Center, P.O. Box 2728, Pittsburgh, PA 15230-2728
43. R. C. Cipolla, APTECH Engineering Services, Inc., 1282 Reamwood Avenue, Sunnyvale, CA 94089
44. R. H. Dodds, Department of Civil Engineering, University of Illinois, 205 North Matthews, Urbana, IL 61801

45. R. Fields, National Institute of Standards and Technology, Building 233, B144, Gaithersburg, MD 20899
46. W. L. Fourney, Department of Mechanical Engineering, University of Maryland, College Park, MD 20742
47. T. J. Griesbach, ATI Consulting, 2010 Crow Canyon Place, Suite 140, San Ramon, CA 94583
48. J. R. Hawthorne, Materials Engineering Associates, 9700B M. L. King, Jr., Highway, Lanham, MD 20706
49. G. R. Irwin, Department of Mechanical Engineering, University of Maryland, College Park, MD 20742
50. L. James, Westinghouse Bettis, P.O. Box 79, West Mifflin, PA 15122
51. J. D. Landes, Department of Engineering Science and Mechanics, 310 Perkins Hall, The University of Tennessee, Knoxville, TN 37996-2030
52. G. R. Odette, Department of Chemical and Nuclear Engineering, University of California, Santa Barbara, CA 93106
53. S. T. Rolfe, Department of Civil Engineering, The University of Kansas, Lawrence, KS 66045-2235
54. A. R. Rosenfield, 1650 Ridgeway Place, Columbus, OH 43212
55. S. T. Rosinski, Department 6741, Sandia National Laboratories, P.O. Box 5800, Albuquerque, NM 87185-5800
56. D. A. Scarth, Ontario Hydro Research Division, 800 Kipling Avenue, Toronto, Ontario, Canada M8A 5S4
57. C. W. Schwartz, Department of Civil Engineering, University of Maryland, College Park, MD 20742
58. E. T. Wessel, 312 Wolverine, Haines City, FL 33844